Jefferson Lab PAC14
Proposal Cover Sheet

This document must be received by close of business Thursday, **June 4, 1998** at:

Jefferson Lab
User Liaison Office,
Mail Stop 12B
12000 Jefferson Avenue
Newport News, VA
23606

Experimental Hall: B
Days Requested for Approval: 15

☒ **New Proposal Title:** A Precision Measurement of the Neutral Pion Lifetime via the Primakoff Effect
☐ **Update Experiment Number:**
☐ **Letter-of-Intent Title:**
(Choose one)

Proposal Physics Goals
Indicate any experiments that have physics goals similar to those in your proposal.

Approved, Conditionally Approved, and/or Deferred Experiment(s) or proposals:

Contact Person
Name: Ashot Gasparian
Institution: Hampton University
Address: Hampton, VA 23668
Address: 115 Sterling ct.
City, State, ZIP/Country: Yorktown, VA 23693
Phone: (757) 766-1031 **Fax:**
E-Mail: gasparian@cebaf.gov

Jefferson Lab Use Only
Receipt Date: 6/4/98
PR 98-105
By: q

BEAM REQUIREMENTS LIST

JLab Proposal No.: 98-105 Date: 6/4/98

Hall: B Anticipated Run Date: _____ PAC Approved Days: _____

Spokesperson: Ashot Gasparian Hall Liaison: B. Mecking
Phone: (727) 269-7323
E-mail: gasparian@cebaf.gov

List all combinations of anticipated targets and beam conditions required to execute the experiment. (This list will form the primary basis for the Radiation Safety Assesment Document (RSAD) calculations that must be performed for each experiment.)

Condition No.	Beam Energy (MeV)	Mean Beam Current (μA)	Polarization and Other Special Requirements (e.g., time structure)	Target Material (use multiple rows for complex targets — e.g., w/windows)	Material Thickness (mg/cm²)	Est. Beam-On Time for Cond. No. (hours)
1	6000	10^{-4}	none	none	—	15
2	6000	10^{-2}	none	Cu	640	144
3	6000	10^{-2}	none	Pb	320	144

The beam energies, E_{Beam}, available are: $E_{Beam} = N \times E_{Linac}$ where N = 1, 2, 3, 4, or 5. E_{Linac} = 800 MeV, i.e., available E_{Beam} are 800, 1600, 2400, 3200, and 4000 MeV. Other energies should be arranged with the Hall Leader before listing.

HAZARD IDENTIFICATION CHECKLIST

JLab Proposal No.: 98-105 (For CEBAF User Liaison Office use only) Date: 6/4/98

Check all items for which there is an anticipated need.

Cryogenics
- ____ beamline magnets
- ____ analysis magnets
- ____ target
  - type: ____
  - flow rate: ____
  - capacity: ____

Electrical Equipment
- ____ cryo/electrical devices
- ____ capacitor banks
- X high voltage
- ____ exposed equipment

Radioactive/Hazardous Materials
List any radioactive or hazadorous/ toxic materials planned for use:
____
____
____
____

Pressure Vessels
- ____ inside diameter
- ____ operating pressure
- ____ window material
- ____ window thickness

Flammable Gas or Liquids
- type: ____
- flow rate: ____
- capacity: ____

Drift Chambers
- type: ____
- flow rate: ____
- capacity: ____

Other Target Materials
- ___ Beryllium (Be)
- ___ Lithium (Li)
- ___ Mercury (Hg)
- X Lead (Pb)
- ___ Tungsten (W)
- ___ Uranium (U)
- ___ Other (list below)

____
____

Vacuum Vessels
- ____ inside diameter
- ____ operating pressure
- ____ window material
- ____ window thickness

Radioactive Sources
- ____ permanent installation
- ____ temporary use
- type: ____
- strength: ____

Large Mech. Structure/System
- X lifting devices
- ____ motion controllers
- ____ scaffolding or
- X elevated platforms

Lasers
- type: ____
- wattage: ____
- class: ____

Installation:
- ____ permanent
- ____ temporary

Use:
- ____ calibration
- ____ alignment

Hazardous Materials
- ___ cyanide plating materials
- ___ scintillation oil (from)
- ___ PCBs
- ___ methane
- ___ TMAE
- ___ TEA
- ___ photographic developers
- ___ other (list below)

____
____

General:

Experiment Class:

- ____ Base Equipment
- ____ Temp. Mod. to Base Equip.
- ____ Permanent Mod. to Base Equipment
- ____ Major New Apparatus

Other: ____
____

LAB RESOURCES LIST

JLab Proposal No.: 98-105 Date 6/4/98

(For JLab ULO use only.)

List below significant resources — both equipment and human — that you are requesting from Jefferson Lab in support of mounting and executing the proposed experiment. Do not include items that will be routinely supplied to all running experiments such as the base equipment for the hall and technical support for routine operation, installation, and maintenance.

Major Installations *(either your equip. or new equip. requested from JLab)*

π^0 detector

New Support Structures: Support for π^0 detector

Data Acquisition/Reduction

Computing Resources:

New Software:

Major Equipment

Magnets: 15 kgm B·dl sweeping magnet downstream of physics target

Power Supplies:

Targets:

Detectors: 1 m x 1 m segmented π^0 detector

Electronics:

Computer Hardware:

Other:

Other:

A Precision Measurement of the Neutral Pion Lifetime via the Primakoff Effect

TJNAF PAC 14 Proposal

June 4, 1998

K. A. Assamagan, L. Gan, A. Gasparian (spokesperson and contact person),
W. Buck, J. Goity, P. Gueye, L. Tang, C. Keppel, K. Baker
Hampton University, Hampton, VA

B. Asavapibhop, R. Hicks, D. Lawrence, R. Miskimen (spokesperson), G. Peterson, J. Shaw
University of Massachusetts, Amherst, MA

A. Ahmidouch, S. Danagoulian (spokesperson), S. Mtingwa, R. Sawafta
North Carolina A&T State University, Greensboro, NC

D. Dale (spokesperson), B. Doyle, T. Gorringe, W. Korsch, C. Popescu,
V. Zeps, P. Zolnierczuk
University of Kentucky, Lexington, KY

E. Chudakoff, R. Ent, M. Ito, B. Wojtsekhowski, J.P. Chen, D. Mack, E. Smith
Thomas Jefferson National Accelerator Facility, Newport News, VA

A. Bernstein, M. Distler, M. Pavan
Massachusetts Institute of Technology, Cambridge, MA

A. Nathan
University of Illinois, Urbana, IL

D. Sober, H. Crannell, A. Longhi
The Catholic University of America, Washington, DC

W. Briscoe, L. Murphy
George Washington University, Washington, DC

I. Aznauryan, H. Egiyan, A. Margaryan, K. Egiyan, S. Stepanyan,
H. Voskanyan, A. Ketikyan, A. Shahinyan, Y. Sharabian, A. Petrosyan
Yerevan Physics Institute, Yerevan, Armenia

A. Glamazdin, A. Omelaenko
Kharkov Institute of Physics and Technology, Kharkov, Ukraine

A. Afanasev
North Carolina Central University, Durham, NC

B. Milbrath
Eastern Kentucky University, Richmond, KY

A.I. Fix, V.A. Tryasuchev
Tomsk Polytechnical University, Tomsk, Russia

Abstract

We propose to perform a precise measurement of the neutral pion lifetime using the small angle coherent photoproduction of the π^o in the Coulomb field of a heavy nucleus, *i.e.* the Primakoff effect. The $\pi^o \rightarrow \gamma\gamma$ decay proceeds primarily via the chiral anomaly and represents one of the most definitive tests of low energy QCD. Presently, higher order corrections to the lifetime, including finite quark mass effects, remain largely untested by experiment. This measurement will be a state-of-the-art experimental determination of the lifetime with a precision of less than 2%, which is commensurate with the theoretical uncertainty. The improved precision is enabled by (1) the use of quasimonochromatic photons from the TJNAF Hall B tagged photon facility and (2), the development of a hybrid π^o detector consisting of a multichannel lead glass detector with a high resolution insertion.

1 Introduction

The two-photon decay mode of the π^o reveals one of the most profound symmetry issues in QCD, namely, the explicit breaking of a classical symmetry by the quantum fluctuations of the quark fields when they couple to a gauge field. This phenomenon, called anomalous breaking, is of a pure quantum mechanical origin. In QCD there are several observable phenomena that originate from such anomalous breakings or anomalies. There is one anomaly connected with the couplings of the quarks to the gluons. This is the so called axial anomaly by which the conservation of the axial U(1) symmetry of the classical Lagrangian of QCD is broken in the limit where two or more quarks are massless, and the divergence of the corresponding axial-vector current becomes proportional to the product $\vec{E}^a \cdot \vec{B}^a$ of the chromoelectric and chromomagnetic fields. The most notorious effect of this anomaly is that there is no SU(3) singlet quasi Goldstone pseudoscalar in the spectrum of mesons. In fact, the lightest such meson is the η' with a large mass of 958 MeV. The origin of this large mass is primarily due to the axial anomaly. The axial anomaly of interest to us involves the coupling to the photons[1][2]. The π^o couples to the isotriplet axial-vector current $\bar{q}\ I_3\ \gamma_\mu\gamma_5\ q$, where $q = (u,\ d)$, and I_3 is the third isospin generator. On the other hand, if we limit ourselves to two quark flavors, the electromagnetic current is given by $\bar{q}\ (1/6 + 1/2I_3)\ \gamma_\mu\ q$. When coupling to the photon, the isosinglet and isotriplet components of the electromagnetic current lead to an anomaly that breaks explicitly the symmetry associated with the axial-vector current $\bar{q}\ I_3\ \gamma_\mu\gamma_5\ q$, and this in turn directly affects the coupling of the π^o to two photons. The decay amplitude is given by:

$$\frac{N_c}{(4\pi F_\pi)^2}\frac{e_{em}^2}{6}\epsilon_{\mu\nu\rho\sigma}k^\mu k'^\nu \epsilon^{*\rho}\epsilon^{*\sigma}, \tag{1}$$

where N_c is the number of colors, k and k' are the photon momenta, and, ϵ and ϵ' are the photon polarizations. As this amplitude depends on the number of colors in QCD, the $\pi^o \to \gamma\gamma$ decay can be used to test that this number is indeed equal to three. The decay rate is then given by:

$$\Gamma(\pi^0 \to \gamma\gamma) = \frac{\alpha_{em}^2 N_c^2 M_\pi^3}{576\pi^3 F_\pi^2}, \tag{2}$$

where $F_\pi \simeq 93$ MeV is the pion decay constant.

The result for the decay amplitude given above is exact in the chiral limit, *i.e.*, when the u- and d-quark masses vanish. In this case, the anomaly is saturated by the π^o pole. However, the current-quark masses in the real world are of the order of 5 MeV. There are two sources of corrections due to this explicit breaking of chiral symmetry. The first, and most important, does not change the form of the amplitude given above. It merely replaces the value of F_π in the chiral limit by the measured value determined from π^+ decay[3]. This is a manifestation of the so-called non-renormalization theorem of the anomaly due to Adler and Bardeen. The second is a correction whose origin is in the contributions to the saturation of the anomaly by excited meson poles (π' for instance). These contributions are suppressed with respect to the π^o contribution by a factor of the order of $M_q/M_{\rm meson}$, where $M_q \simeq 5$ MeV is the light quark mass. In Chiral Perturbation Theory such corrections manifest themselves through terms of negative intrinsic parity of order p^6 in the effective Lagrangian. These

terms in the Lagrangian have effective coupling constants that cannot be known a priori, and therefore theory cannot predict these corrections. A measurement of $\Gamma(\pi^0 \to \gamma\gamma)$ with an error of 2% or less, as proposed here, is expected to be extremely useful in illuminating the chiral symmetry breaking corrections due to quark masses[4][5]. In fact, the error in the amplitude (1) is expected to be a few parts in a thousand. Any observed deviation from it will be due to the p^6 terms mentioned above. The size of such terms have been calculated in a Nambu-Jona-Lasinio type of model[6]. The authors find a $4.0^{+2.7}_{-1.6}$% correction to the π^o width. An effect of this magnitude would be accessible to the experiment proposed here.

2 Previous experiments

The present experimental knowledge of the π^o width is summarized in figure 1 [7][8]. Three general experimental techniques have been used to access the neutral pion width: the direct method, $\gamma\gamma$ collisions, and the real Primakoff effect. In addition, a future experiment planned for Hall A of TJNAF [9] will measure the slope of the pion form factor $F_{\gamma\gamma^*\pi^o}(q^2)$ at low q^2 using the small angle scattering capabilities of the Hall A Møller polarimeter.

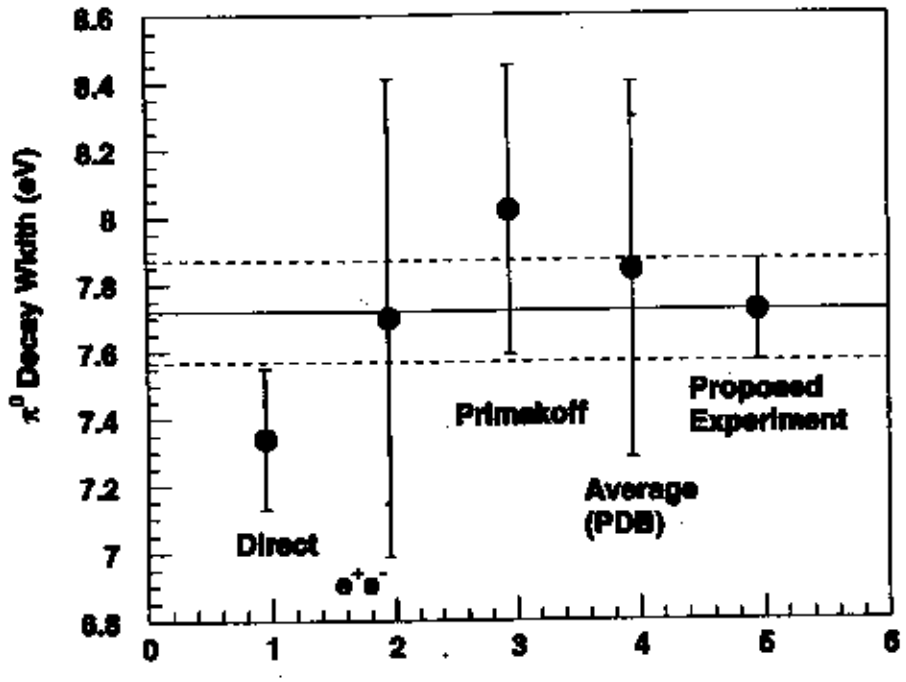

Figure 1. $\pi^o \to \gamma\gamma$ decay width in eV. The horizontal line is the prediction of the chiral anomaly with an estimated 2% error [7]. The experimental results with errors are for : 1) the direct method [11]; 2) e^+e^- [13]; 3) the Primakoff method [15]; 4) Particle Data Book Average [8]; 5) the expected result for the proposed experiment.

2.1 The direct method

Direct measurement of the π^o lifetime has proven difficult due to the large energies and/or high spatial resolution required. In order to be able to discern distinct production and decay points of the π^o, one must take advantage of relativistic time dilation to get the pion to survive long enough in the laboratory frame. Additionally, good knowledge of the spectrum of the produced pions is necessary in order to extract the lifetime via this method.

The first measurement utilizing such a technique was performed at the CERN PS in 1963 [10]. The precision achieved was 17%. In 1985, an improved version of this technique was employed at the CERN SPS whereby a pion lifetime of $\tau_{\pi^o} = (0.897 \pm 0.022 \pm 0.017) \times 10^{-16}$ seconds was obtained [11], corresponding to a width of $\Gamma_{\pi^o} = (7.34 \pm 0.18 \pm 0.11)$ eV. In this experiment, a 450 GeV/c proton impinged upon two tungsten foils whose separation was variable. The first foil served as the π^o production target and the second foil converted the π^o decay photons to electron-positron pairs. The positrons were subsequently detected. For a small foil separation, some of the π^o's decayed after the second foil, whereas for a large distance between the foils, essentially all of the π^o's decayed before the second foil. Thus, by measuring the positron rates for three different foil spacings ranging from 5 to 250μm, the authors were able to determine the lifetime. The dominant systematic errors arise from uncertainties in the π^o spectrum which was assumed to be the arithmetic mean of the π^+ and π^- spectra. In addition, corrections had to be made for the Dalitz decay of the π^o's, conversion of the photons in the π^o production target, prompt positron and photon production, and positrons from the decay of η's.

It is interesting to note that this experiment, the most precise of those performed to date, is not in agreement with the chiral anomaly prediction[12]. As such, this experiment provides impetus for a more precise measurement employing a different technique.

2.2 Measurements using $\gamma\gamma$ collisions

The π^o width has been measured using electron-positron collisions at DESY via $e^+e^- \rightarrow e^+e^-\gamma^*\gamma^* \rightarrow e^+e^-\pi^o \rightarrow e^+e^-\gamma\gamma$ [13]. The incident leptons are scattered at very small angles, and are not detected in the final state. In so doing, they radiate quasireal photons which couple to the π^o which is subsequently identified in an invariant $\gamma\gamma$ mass spectrum. The photons were detected using the Crystal Ball detector which consists of a large array of NaI(Tl) crystals providing 93% solid angle coverage.

The resulting width so obtained was $\Gamma_{\pi^o} = (7.7 \pm 0.5 \pm 0.5)$ eV (see figure 1). Contributions to the systematic error included luminosity normalization, detector efficiencies, cosmic ray rejection, and beam-gas collisions. The latter effect arises from the production of π^o's via the interaction of the leptons with residual gas in the beam pipe.

2.3 Measurements using the Primakoff effect

The Primakoff effect, *i.e.* photopion production off the Coulomb field of a nucleus (see figure 2), has been used in a number of experiments to study the π^o lifetime [14, 15, 16, 17, 18]. The production of π^o's in the Coulomb field of a nucleus by real photons is essentially the

inverse decay $\pi^o \rightarrow \gamma\gamma$, and the cross section for this process thus provides a measure of the pion lifetime.

Using bremsstrahlung beams of energy 4.4 GeV and 6.6 GeV at Cornell, Browman, *et al.* [15] measured the Primakoff cross sections on several nuclei and obtained a total decay width of $\Gamma_{\pi^o} = (8.02 \pm 0.42)$ eV. As pointed out in [7] and [13], however, the quoted error bar may in fact be an underestimate, as an analogous measurement of the η width using the Primakoff effect employing a very similar experimental setup and analysis techniques is not in agreement with other experiments.

In view of both the strong theoretical interest in the subject as well as the recent availability of high intensity, high energy tagged photon beams in Hall B of TJNAF, a high precision, state-of-the-art measurement of the π^o lifetime is desirable. In particular, the Hall B tagged photon facility will enable a measurement which will hold two distinct advantages over previous measurements involving bremsstrahlung beams: (1) the quasimonochromatic nature of the tagged beam will enable a clean kinematical separation of the Primakoff mechanism from various background processes, and (2) the tagging technique will enable significantly better control over systematic errors associated with the photon flux normalization.

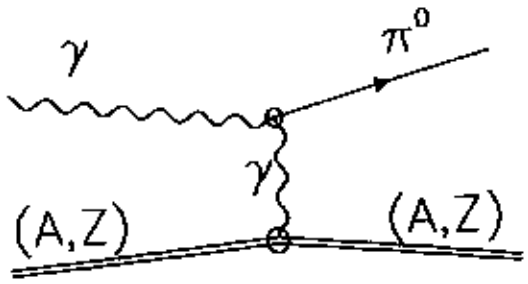

Figure 2. Schematic representation of the Coulomb photoproduction of neutral pions (Primakoff effect).

3 The proposed experiment

We propose to use the quasimonochromatic photons of energy 5.1–5.7 GeV from the Hall B photon tagging facility to measure the absolute cross section of small angle π^o photoproduction off the Coulomb field of complex nuclei. The invariant mass and angle of the pion will be reconstructed by detecting the π^o decay photons from the $\pi^o \rightarrow \gamma\gamma$ reaction.

For unpolarized photons, the Primakoff cross section is given by[16]:

$$\frac{d^3\sigma_P}{d\Omega} = \Gamma_{\gamma\gamma}\frac{8\alpha Z^2}{m^3}\frac{\beta^3 E^4}{Q^4}|F_{e.m.}(Q)|^2 \sin^2\theta_\pi \qquad (3)$$

where $\Gamma_{\gamma\gamma}$ is the pion decay width, Z is the atomic number, m, β, θ_π are the mass, velocity and production angle of the pion, E is the energy of incoming photon, Q is the momentum

transfer to the nucleus, $F_{e.m.}(Q)$ is the nuclear electromagnetic form factor, corrected for absorption of the outgoing pion.

As the Primakoff effect is not the only mechanism for pion photoproduction at high energies, some care must be taken to isolate it from competing processes. In particular, the total cross section is given by:

$$\frac{d^2\sigma}{d\Omega_\pi} = \frac{d\sigma_P}{d\Omega} + \frac{d\sigma_C}{d\Omega} + \frac{d\sigma_I}{d\Omega} + 2 \cdot \sqrt{\frac{d\sigma_P}{d\Omega} \cdot \frac{d\sigma_C}{d\Omega}} cos(\phi_1 + \phi_2) \tag{4}$$

where the Primakoff cross section, $\frac{d\sigma_P}{d\Omega}$, is given by equation (3). The nuclear coherent cross section is given by:

$$\frac{d\sigma_C}{d\Omega} = C \cdot A^2 |F_N(Q)|^2 sin^2\theta_\pi \tag{5}$$

and the incoherent cross section is:

$$\frac{d\sigma_I}{d\Omega} = \xi A(1 - G(Q)) \frac{d\sigma_H}{d\Omega} \tag{6}$$

where A is the nucleon number, $Csin^2\theta_\pi$ is the square of the isospin and spin independent part of the neutral meson photoproduction amplitude on a single nucleon, $|F_N(Q)|$ is the form factor for the nuclear matter distribution in the nucleus, corrected for absorption of the outgoing pion, ξ is the absorption factor of the incoherently produced pions, $1 - G(Q)$ is a factor which reduces the cross section at small momentum transfer due to the Pauli exclusion principle, and $\frac{d\sigma_H}{d\Omega}$ is the π^o photoproduction cross section on a single nucleon. The relative phase between the Primakoff and nuclear coherent amplitudes without absorption is given by ϕ_1 and the phase shift of the outgoing pion due to absorption in the final state is given by ϕ_2.

Kinematical considerations enable one to separate Primakoff from other photopion production mechanisms. The Primakoff cross section is zero for pions emitted along the incident photon direction, has a sharp maximum at an angle $\theta_\pi \sim m_\pi^2/2E_\pi^2$, and falls rapidly to zero at larger angles. It is proportional to Z^2, and its peak value is roughly proportional to E^4. The nuclear coherent cross section is also zero in the forward direction, has a broad maximum outside the angular region of the Primakoff effect, and falls at larger angles as shown in figure 3, where the amplitudes are taken from reference [15] and distortion effects are not included. It is expected to vary little with energy [16]. Consequently, this experiment requires a π^o detector with good angular resolution to eliminate nuclear coherent production, and good energy resolution in the decay photon detection will enable an invariant mass cut to suppress multiphoton backgrounds.

4 Experimental setup

The primary experimental equipment required in the proposed experiment includes: (1) the Hall B photon tagger; (2) a sweeping magnet located after the tagging dipole; (3) 5% r.l. solid π^o production targets (Pb and Cu); (4) a 1m × 1m highly segmented lead glass photon detector for π^o decay photons, with a high resolution insertion in the central region near the

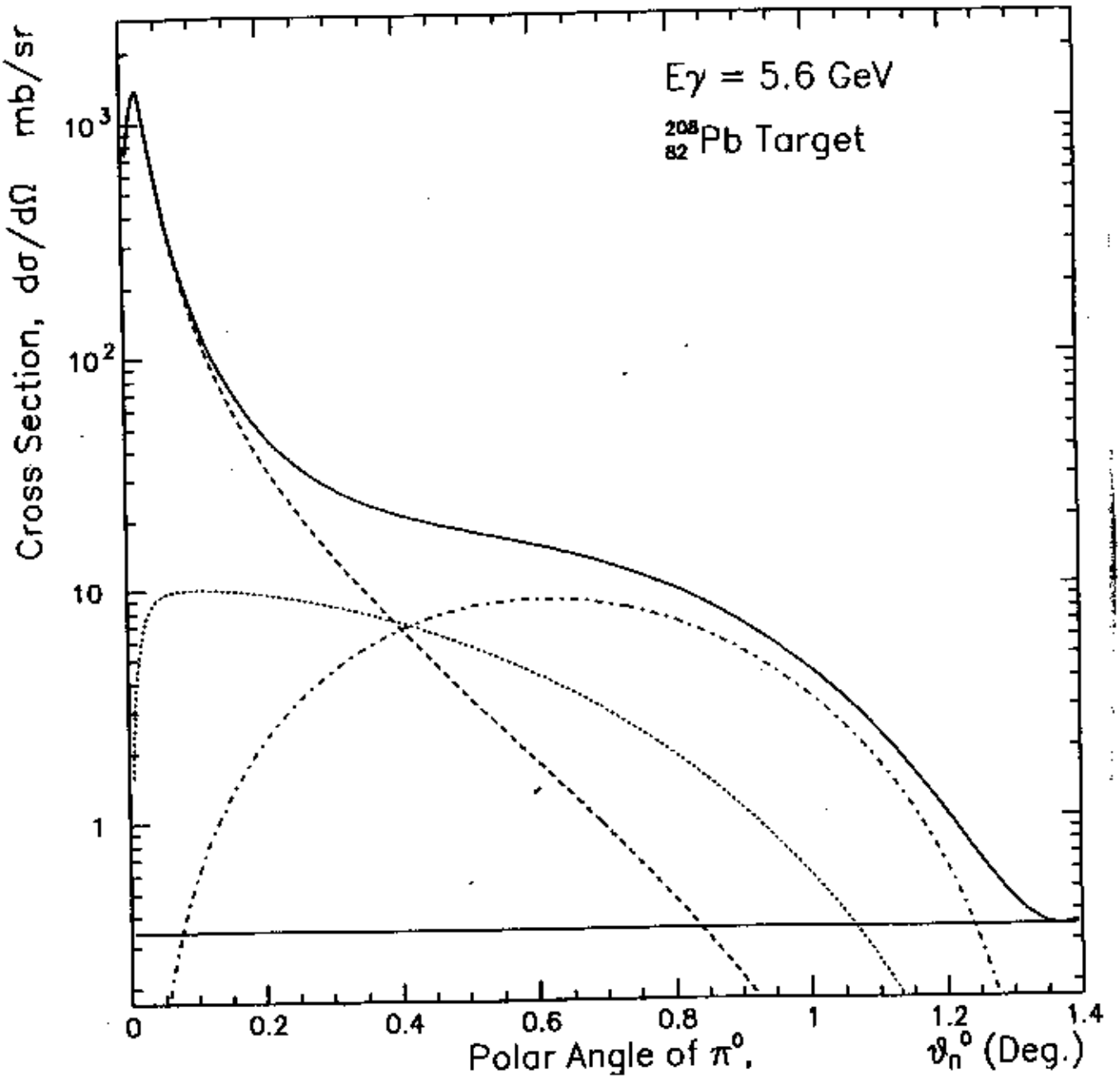

Figure 3. Angular behavior of the electromagnetic and nuclear cross sections for ^{208}Pb in the 6.0 GeV energy range. The various curves are: dashed — Coulomb; dash-dotted — nuclear coherent; dotted — electromagnetic and nuclear interference; long-dashed — nuclear incoherent.

beam and a plastic scintillator charged particle veto. To reduce charged electromagnetic backgrounds a second sweeping dipole will be located after the π^o production target. (See figure 4)

4.1 Photon tagging

The primary advantages of the experiment being proposed here over the previous Primakoff experiments [15, 16, 17, 18] arise from the possibility of using the TJNAF Hall B tagging facility to carefully control systematic errors and reduce backgrounds. First, it is clear that the tagging technique will enable a significantly more accurate knowledge of the photon flux. We estimate that it can be controlled to better than 1% by taking the steps discussed below. Second, due to the strong energy dependence of the Primakoff cross section (E^4), it is critical to have a good knowledge of the absolute photon beam energy. In the untagged case of reference [15] it was known to 0.5% and created a 3% uncertainty in the decay width. We anticipate a factor of five improvement in the energy uncertainty at TJNAF.

We propose to use a 6 GeV electron beam incident on a thin (10^{-3}–10^{-4} r.l.) bremsstrahlung converter foil. The post-bremsstrahlung electrons will be momentum analyzed in the Hall B photon tagger dipole magnet [19], and photons will be tagged in the energy range 5.1 to 5.7 GeV. (See figure 5). To minimize background hits in the tagger that can lead to false photon triggers and overestimates of the photon flux, we plan to run with both the "T" and "E" counters in the focal plane and require a triple coincidence of the left and right photomultiplier tubes of the "T" counter and the corresponding "E" counter. Running with the "E" counters also has the advantage of better energy resolution (0.1%) as compared to the "T" counters alone (1%). To determine the absolute photon flux, we plan to periodically (approximately once per day) remove the target and insert a lead glass detector at the target position and a 2×10^{-5} radiation length radiator in the bremsstrahlung converter position. Data will be taken triggered on the tagger Master OR (MOR) with the beam current reduced to approximately 0.1 nA. The tagging efficiency will thus be given by (Lead Glass·MOR)/MOR. Relative measurements of the photon flux will be made with the pair spectrometer and pair counter located in the Hall B alcove. We also plan to look at electron-positron pairs from photon conversion in the target as an absolute measure of the luminosity. The sweeping magnet downstream of the target will deflect the e^+e^- pairs away from the detector array and into scintillator paddles located to the left and right of it. The scalers for these devices will be read out during normal data taking, giving real time flux and luminosity measurements.

To reduce uncertainties in the photon flux due to beam positioning, steering, and collimator alignment, we propose to run with the photon collimators removed from the beamline. Since our target is close to the photon radiator and the divergence of the photon beam is small due to the 6 GeV electron beam energy, the collimators are expected to add little to the measurement and may introduce systematic errors in the flux normalization. The photon beam will be steered into Hall B by centering it on a one centimeter scintillator located approximately 50 meters downstream of the radiator in the Hall B alcove. This scintillator should be accurately surveyed and placed on the beamline center.

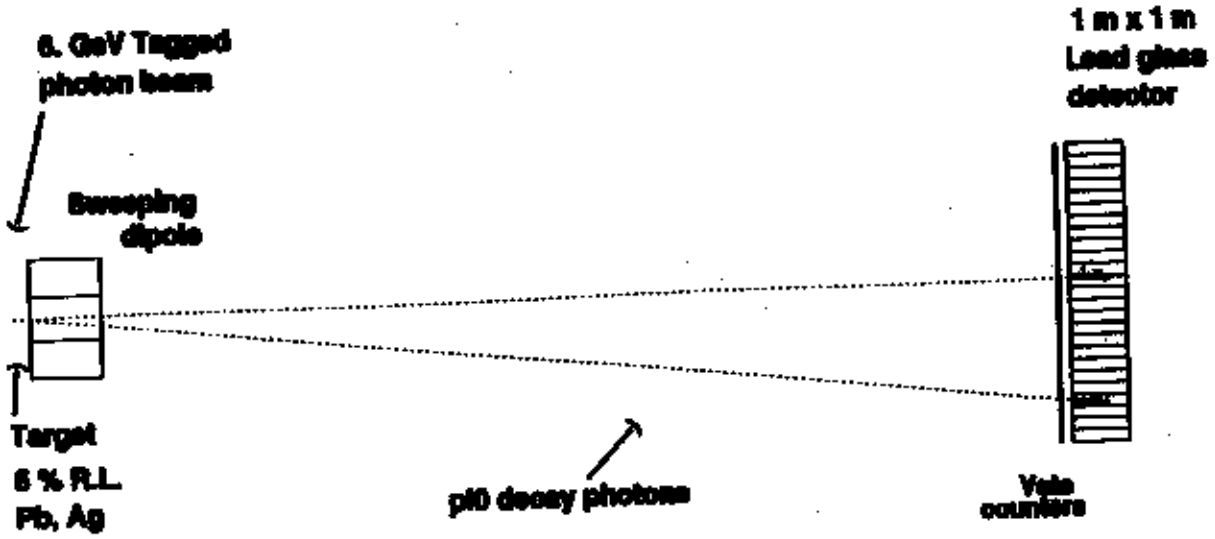

Figure 4. Layout of the experimental setup (side view).

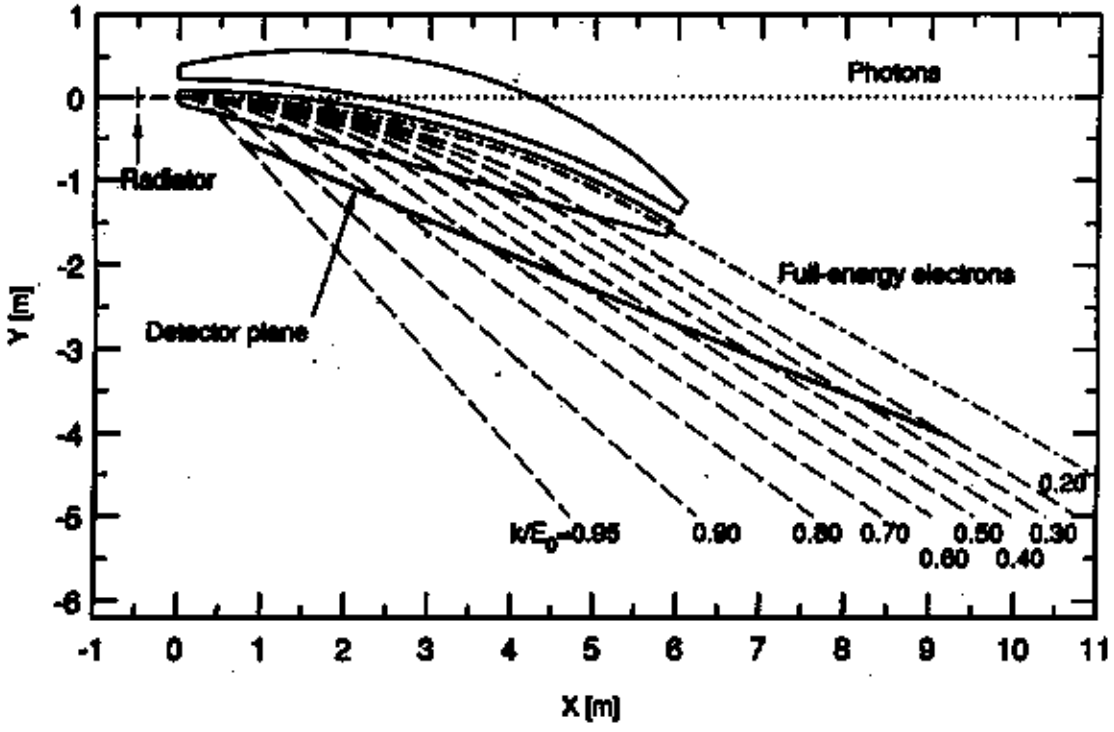

Figure 5. Side view of the Hall B photon tagging system. (Figure is from [19]).

4.2 The π^o detectors

We propose to use a segmented array of lead glass Cherenkov detectors (see figure 6), a 25×25 matrix 1m × 1m in size, situated 7.5 meters downstream of the π^o production target to detect the π^o decay photons. Each lead glass module will be 4cm × 4cm × 40cm, with a total of 504 channels[23]. In addition, we propose to build an array of 2 cm × 2 cm × 20 cm $PbWO_4$ crystal detectors[20] in the central region of the array covering 44 cm × 44 cm for enhanced coordinate and energy resolution in the region near the beam where photons from the $\pi^o \to \gamma\gamma$ decay are of higher energy. The addition of the high resolution insertion will significantly improve the invariant mass and angle reconstruction of the pions. In order to control the coordinate and energy resolutions, a multichannel light monitoring system will also be employed.

The central 6 cm × 6 cm area will be left open to enable the photon beam to pass through. The modules contiguous with this region on the beam axis as well as the modules on the outer boundaries of the lead glass wall will be excluded from the fiducial volume of the detector to control coordinate resolution and detection efficiency. Figure 7(a) shows the distribution of photons under the condition that both of the π^o decay photons hit the physical size of the detector. This corresponds to a geometrical acceptance of 82%. Figure 7(b) indicates the distribution when both photons hit the face of the detector when the central region and the adjacent central blocks are excluded. This cuts the geometrical π^o acceptance to 74%. Figure 7(c) is the hit pattern for the case when each of the photon pair hits the fiducial volume of the detector (*i.e.* with the central blocks and all of the blocks on the outermost boundary excluded). The additional exclusion of the outermost blocks has little effect on the acceptance, as it is reduced to only 73%. Figure 7(d) corresponds to the hit pattern on the entire fiducial volume (as in Figure 7(c)), with the added constraint that the sum of the energy deposition of the two photons exceeds 4 GeV and any given photon deposits at least 0.2 GeV. The additional energy cut has little effect on the geometrical acceptance as it remains at 73%. In order to increase count rates, and to minimize systematic errors associated with correcting for finite acceptance effects, it is clearly desirable to have a large π^o acceptance. As figure 7 indicates, the main limitation on the acceptance arises from the exclusion of the central modules. Simulations show that excluding an additional ring of blocks (16 in number) around the central region gives an additional factor of about two reduction in acceptance. This places a limitation on how far downstream the detector may be placed from the bremsstrahlung converter. It should be noted in this regard, however, that the smaller Molière radius of the $PbWO_4$ crystals in the central region enables one to extend the fiducial volume of the detector closer to the beamline, thereby increasing the area of coverage in the important central region of the detector.

Figure 8 illustrates the optimum separation between the π^o production target and the lead glass detector. For small separations, approximately 5 meters or less, the π^o detection efficiency falls as a significant number of photons cross the plane of the detector at distances too close to the central axis, and thus do not intersect the fiducial volume. At large separations of the production target and photon detector, the geometrical acceptance falls as photons intersect the plane of the detector outside its outer boundary.

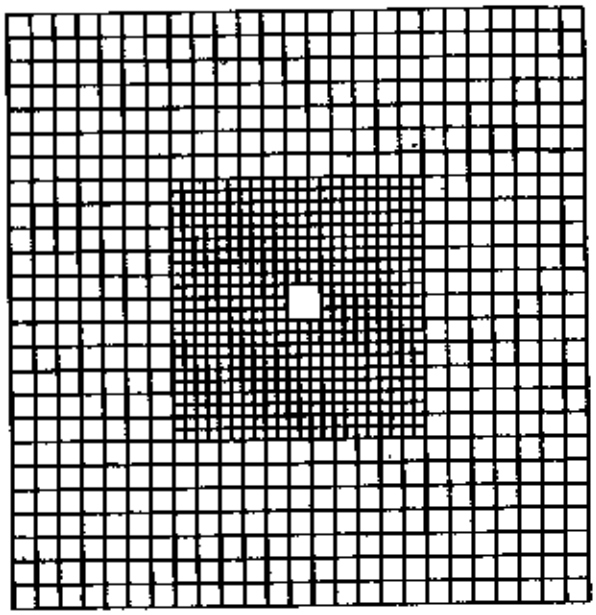

Figure 6. Schematic representation of the proposed hybrid photon calorimeter. The central blocks will be 2 cm × 2 cm $PbWO_4$ crystals and the outer blocks are 4 cm × 4 cm lead glass blocks.

As indicated in figure 3, one would like to have a large, flat acceptance in θ_π out to at least two degrees to verify that the effect of the coherent nuclear photoproduction amplitude is taken into account adequately. Figure 9 shows the π^o geometrical acceptance as a function of θ_π where this is seen to be the case.

We propose to place a sweeping magnet ($\int B \cdot dl \sim 15$ kilogauss m) just downstream of the target to sweep charged particles away from the π^o detector. In addition, we plan to install a helium bag between the target and the detector to minimize backgrounds. Figure 10 shows the expected power incident on the the detector modules which lie in the dispersive (*i.e.* horizontal) plane of the sweeping magnet at the beam height.

4.3 Resolutions

Particle identification of the pions will be accomplished by calculating the invariant mass of coincident photon pairs from the experimentally measured quantities E_{γ_1}, E_{γ_2}, and $\psi_{\gamma_1\gamma_2}$, the opening angle between the two photons. The square of the invariant mass is given by:

$$m^2_{\pi^o} = 2E_{\gamma_1}E_{\gamma_2}(1 - cos\psi_{\gamma_1\gamma_2}). \tag{7}$$

Good invariant mass resolution is needed to minimize uncertainties associated with background subtractions. Figure 11 shows the expected invariant mass resolution of our setup

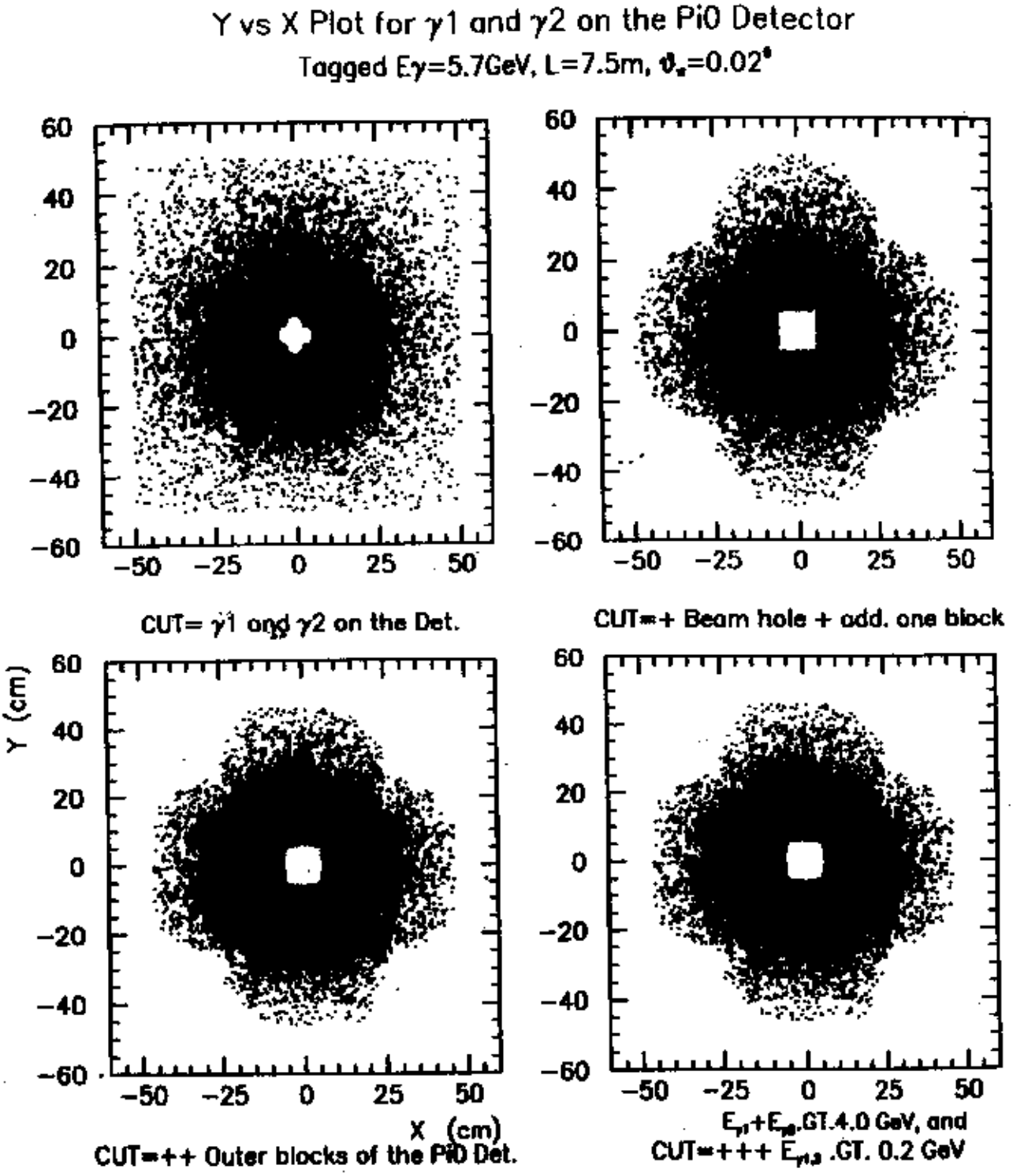

Figure 7. Monte Carlo distribution of two gamma events from π^o decay on the detector for different cut parameters (see text for details).

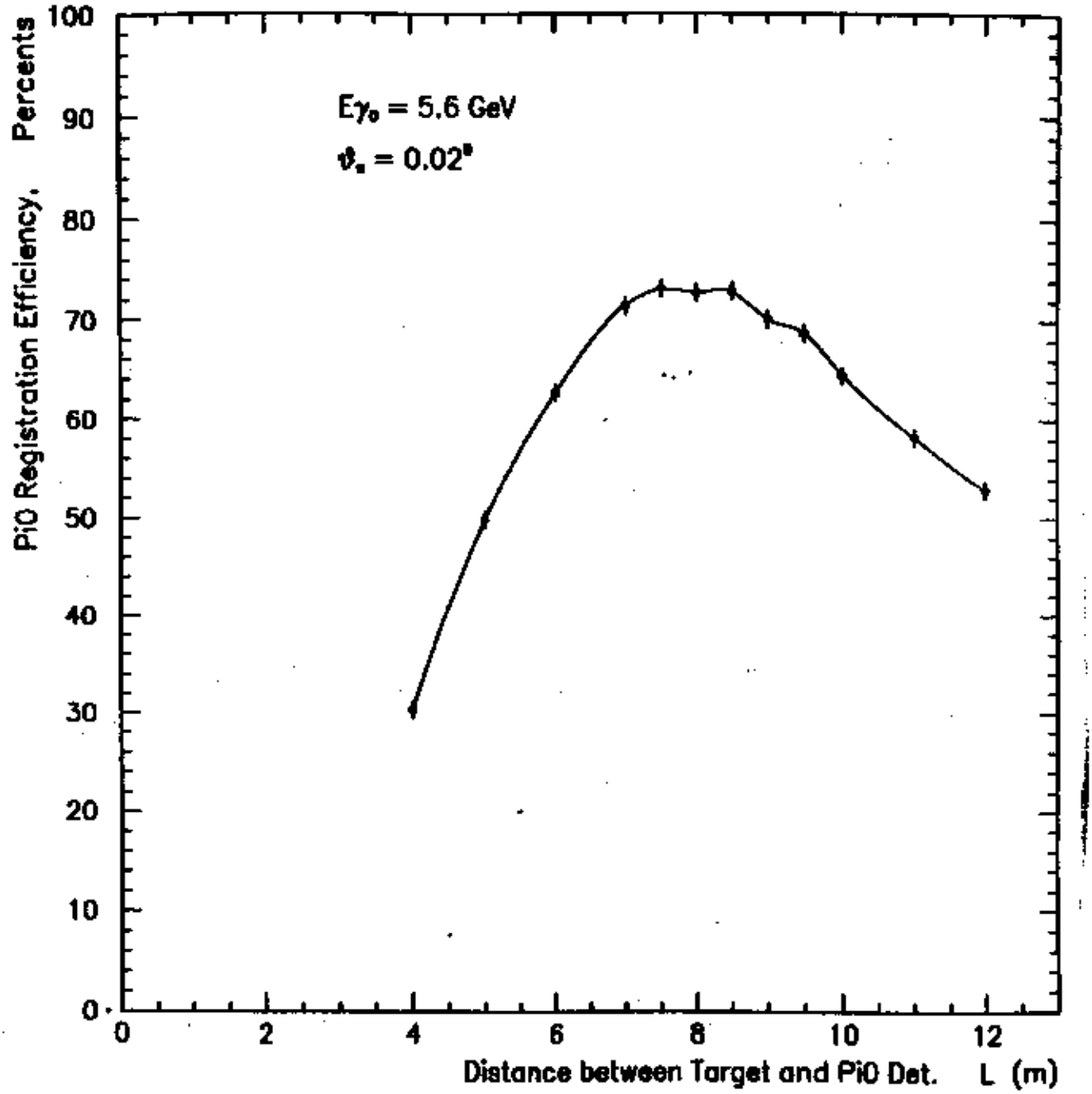

Figure 8. π^o detection efficiency *vs.* distance between the target and photon detector.

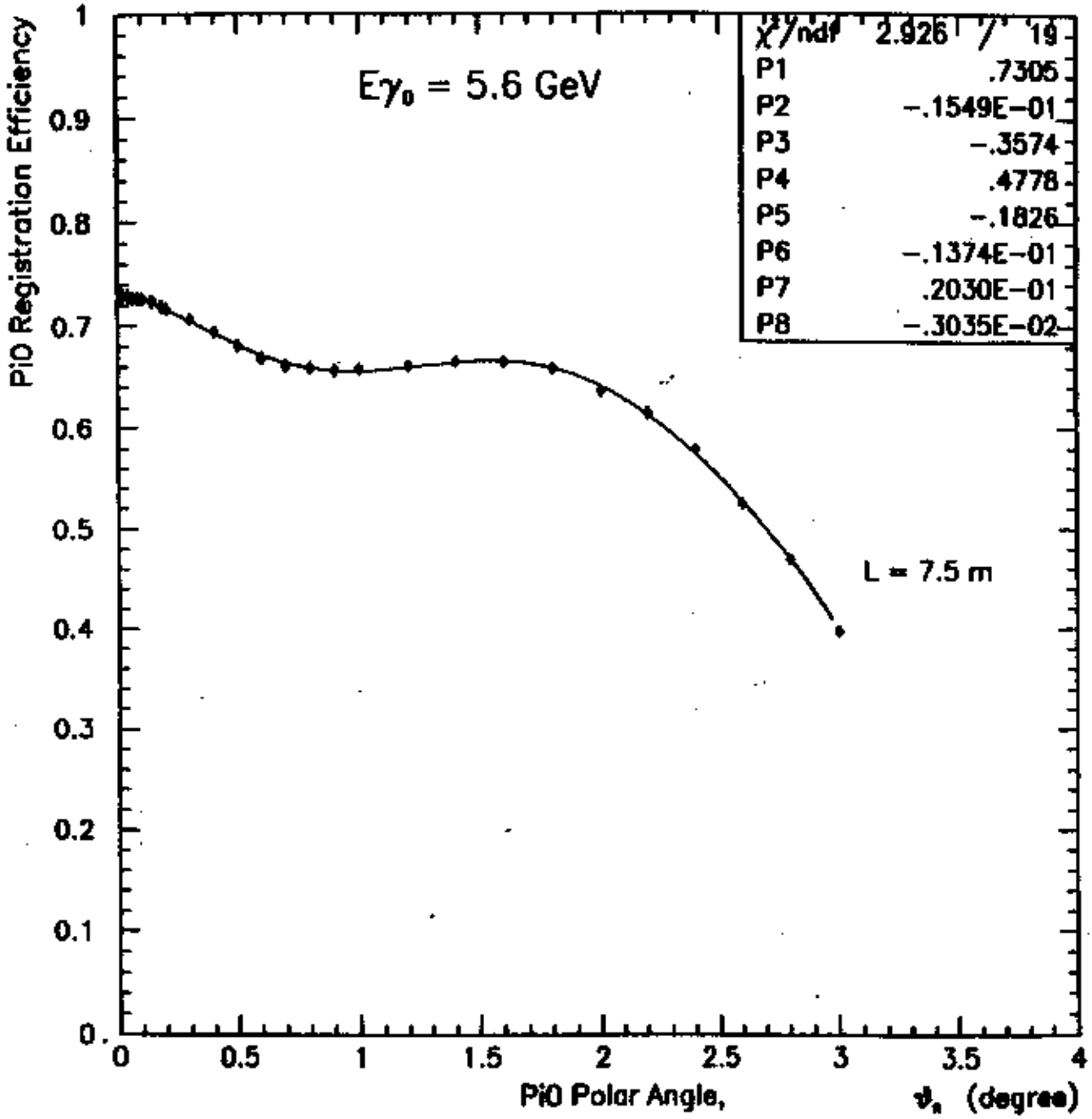

Figure 9. π^0 detection efficiency *vs.* production angle. The distance between target and detector is 7.5 m.

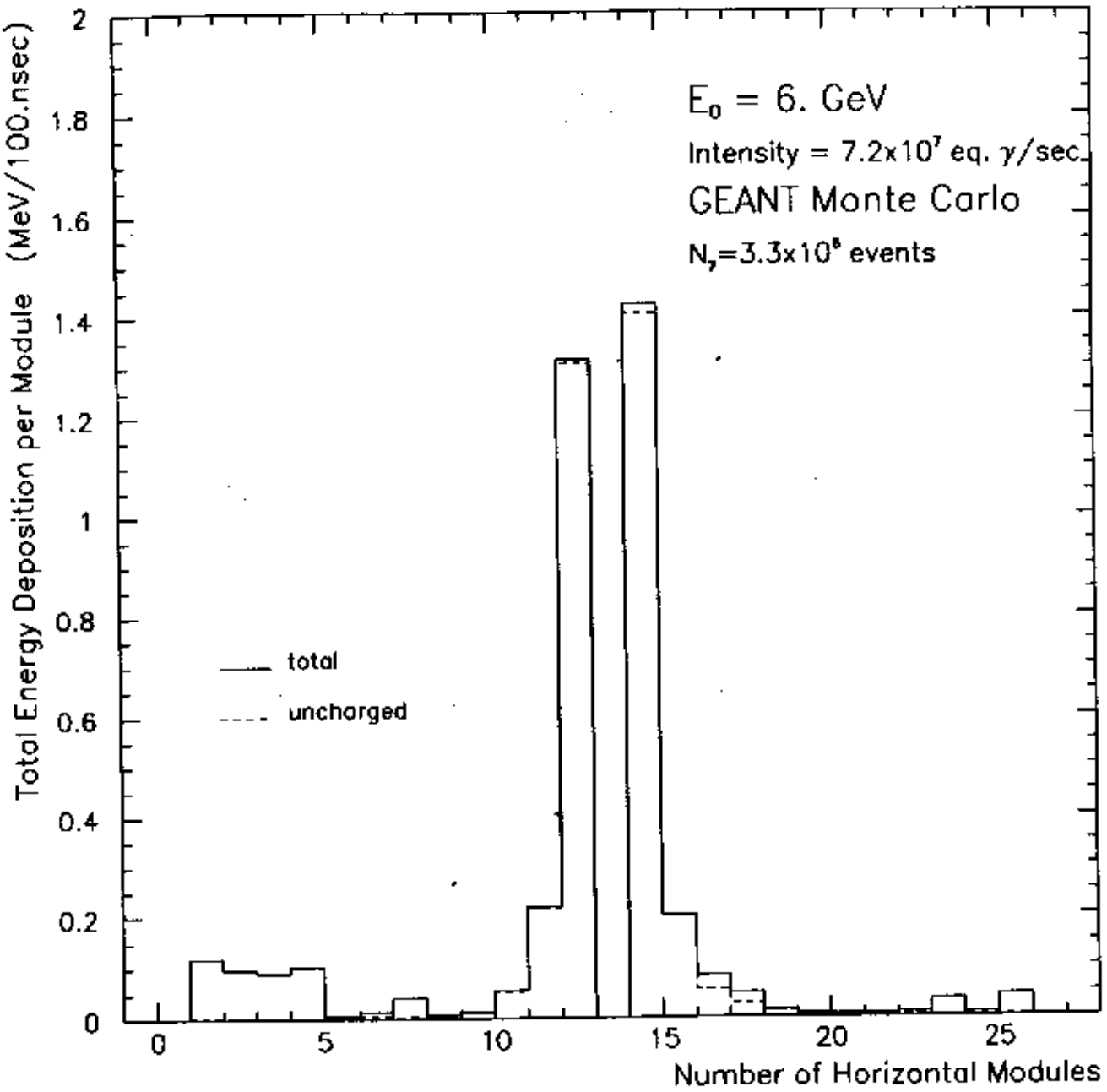

Figure 10. Energy deposition along the horizontal row of detector modules at the beam height. Dashed line is uncharged particles; solid line is charged + uncharged.

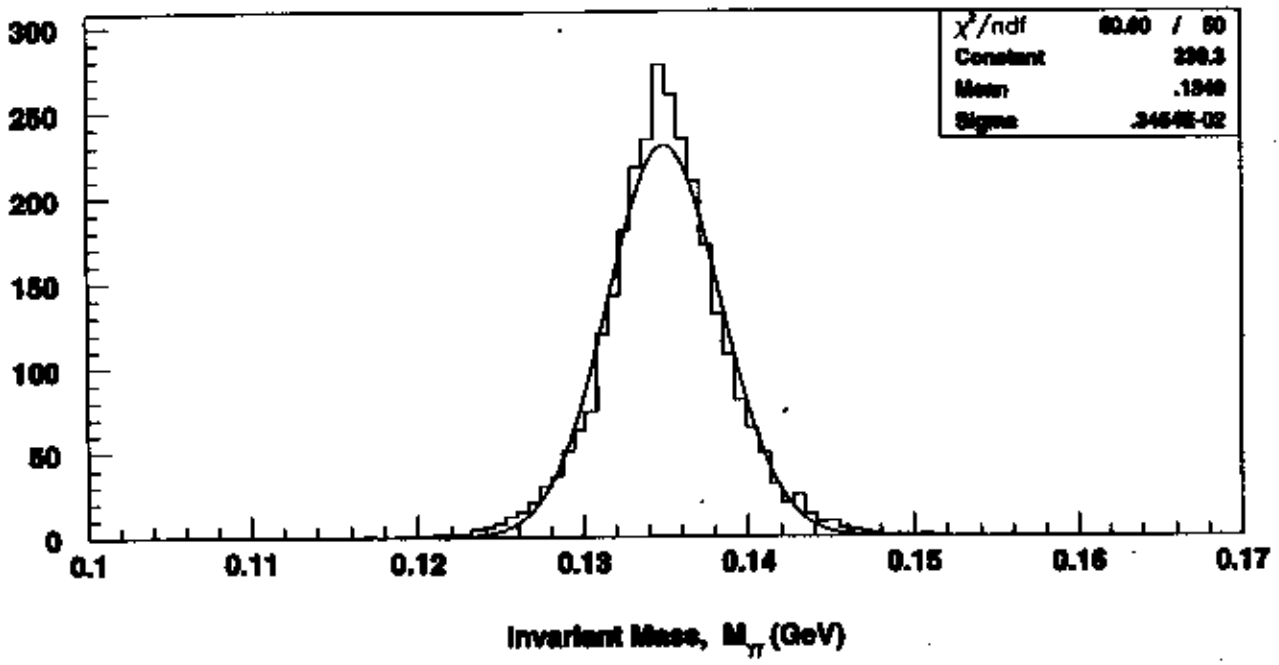

Figure 11. The $M_{\gamma\gamma}$ invariant mass distribution.

for coherent pion production on lead for $E_\gamma = 5.7$ GeV$\pm$0.3% and $\theta_{\pi^o} = 0.1°$, where it can be seen that we expect an experimental resolution of about 3.5 MeV. A number of techniques for determining the pion energy with the proposed hybrid detector have been examined[21]. The first and crudest method involves simply summing the experimentally measured energies of the two photons. The results of this method are shown in figure 12(a). For the online data analysis, this method will be implemented in the first energy cut on the raw data.

A second method involves the use of the energy sharing between the two photons and the opening angle provided by the experimentally measured coordinate information:

$$E_{\pi^o} = \sqrt{\frac{2m_{\pi^o}^2}{(1-X^2)(1-cos\psi_{\gamma_1\gamma_2})}}, \tag{8}$$

where

$$X = (E_{\gamma 1} - E_{\gamma 2})/(E_{\gamma 1} + E_{\gamma 2}). \tag{9}$$

The results of this method for our detector with the high resolution insertion are shown in figure 12(b), where it can be seen that only marginal improvement is obtained. In general, this method is best suited for photon detectors of poor energy resolution and good angular resolution.

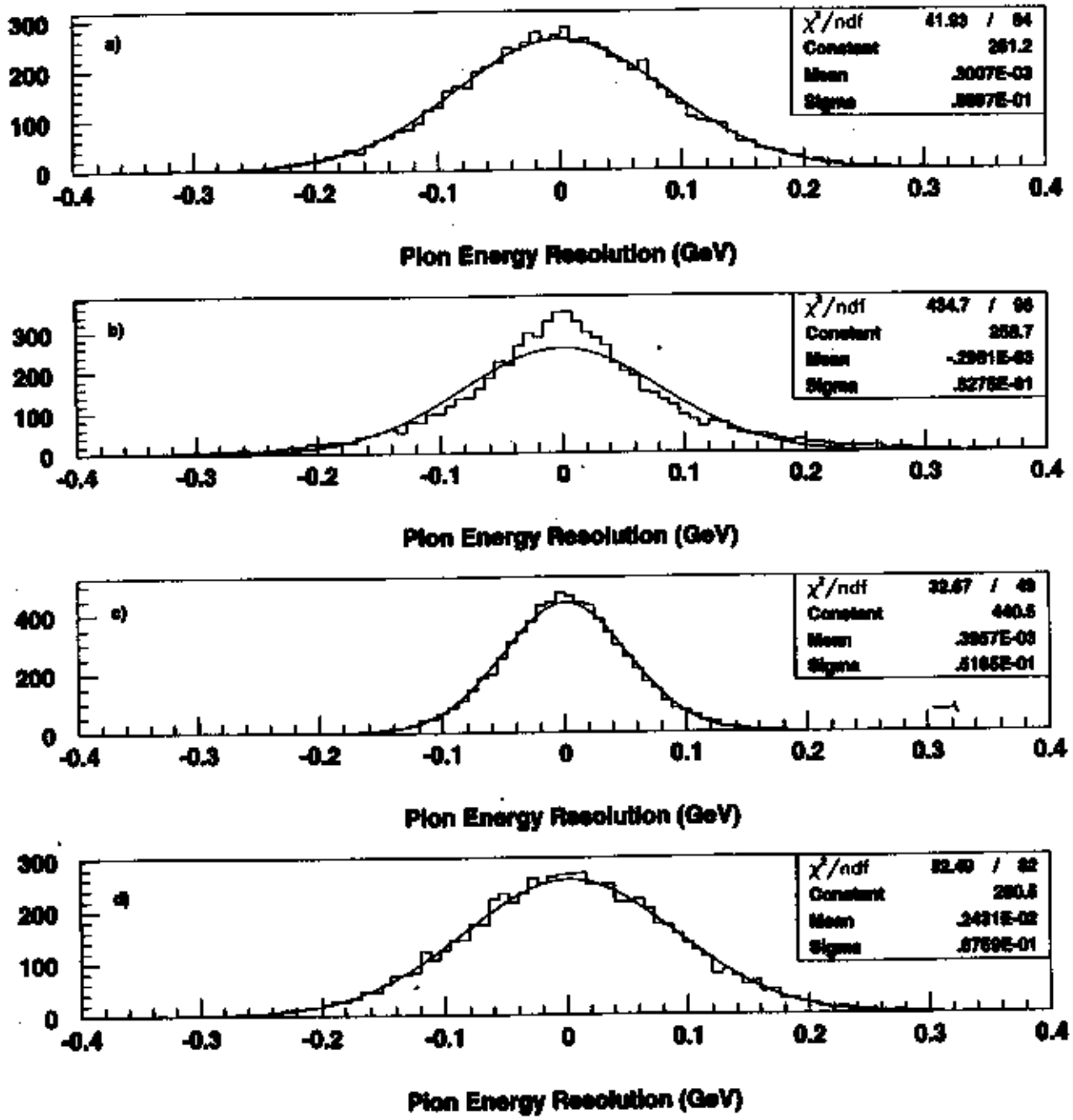

Figure 12. π^o energy resolution for different methods of determining the pion energy. Distribution of events *vs.* $(E_{\pi^o}^{sampled} - E_{\pi^o}^{reconstructed})$ for a) sum of energies; b)energy sharing technique; c)using energy and opening angle; d) same as method (c), but without the high resolution detector insertion.

The energy can also be reconstructed using the the measured energy of one of the photons and the opening angle:

$$E_{\pi^o} = E_{\gamma i} + \frac{m_{\pi^o}^2}{2E_{\gamma i}(1 - cos\phi_{\gamma_1\gamma_2})}. \tag{10}$$

The results of this third method are shown in figure 12(c). As is seen from the figure, the resolution is considerably improved. This is a result of the fact that in most cases the higher energy photon is registered in the high resolution insertion of the detector where coordinate and energy resolution are each a factor of two better than in lead glass. By comparison, if one were to measure the pion energy by the same method but without the high resolution insertion, one obtains a significantly degraded resolution as evidenced in figure 12(d).

Resolution in θ_{π^o} is of particular importance in the identification of the forward peaked π^o's photoproduced by the Primakoff mechanism ($\theta_{\pi^o} \sim 0.04°$) from pions produced at larger angles via the nuclear field (see figure 3). The pion angle can be determined from the measured photon energies and angles by:

$$cos\theta_{\pi^o} = \frac{E_{\gamma 1}cos\theta_{\gamma 1} + E_{\gamma 2}cos\theta_{\gamma 2}}{\sqrt{E_{\gamma 1}^2 + E_{\gamma 2}^2 + 2E_{\gamma 1}E_{\gamma 2}cos\psi_{\gamma 1\gamma 2}}}. \tag{11}$$

Figure 13(a) shows the expected angular resolution for coherently produced pions for $E_\gamma = 5.7 \pm 0.3\%$ and $\theta_{\pi^o} = 0.1°$ for a detector consisting of lead glass blocks only. Figure 13(b) shows the improved resolution by implementing the high resolution detector insertion.

The angular resolution under the Primakoff peak can be further improved by means of a kinematical fit, the results of which are shown in figure 13(c). If the incident photon energy is known, and the residual nucleus is left in its ground state as is the case with coherently photoproduced pions, a correlation between the opening angle and the two photon energies results. This correlation is shown in figure 14(a), and the projection onto the $\psi_{\gamma\gamma}$ axis, figure 14(b), gives the opening angle distribution. This additional kinematical constraint results in the improved angular resolution in figure 13(c).

A further consideration in θ_{π^o} resolution involves the accuracy of which the interaction vertex is known. Figure 15(a) shows the calculated angular resolution for a pointlike photon beam spot size on the target. Figures 15(b) and 15(c) show, respectively, the progressive degradation in resolution for four and ten millimeter spot sizes. Such considerations argue for a placement of the target as close to the bremsstrahlung converter as is practical, while still providing space for sweeping magnets. We propose placing the π^o production target 7 meters downstream of the converter. In order to get good acceptance for pions, this requires that the π^o detector be placed upstream of the CLAS, 14 meters from the bremsstrahlung converter.

5 Count rate estimates and beamtime

A Monte Carlo generation of the events has been done for several nuclear targets. In these simulations all amplitudes contributing to this process were used normalized to the available experimental data for E_γ=6.6 GeV [15]. The expected experimental yields in six day runs for 5% r.l. copper and lead targets are shown in figures 16 and 17, respectively. The errors

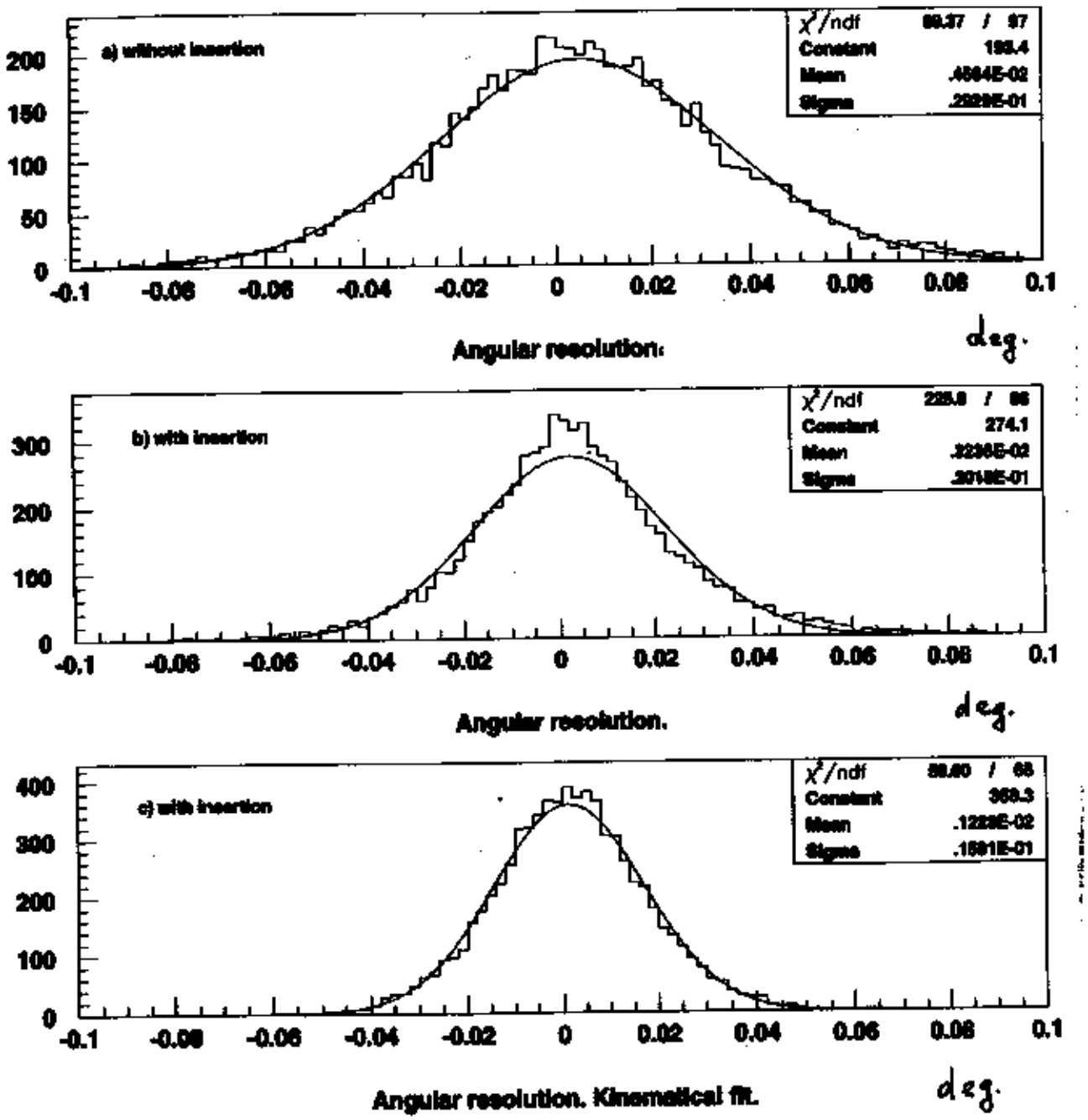

Figure 13. π^o angular resolution. Distribution of events *vs.* $(\theta_{\pi^o}^{sampled} - \theta_{\pi^o}^{reconstructed})$ a) without high resolution insertion; b) with high resolution detector insertion; c) with high resolution detector insertion and kinematical fit.

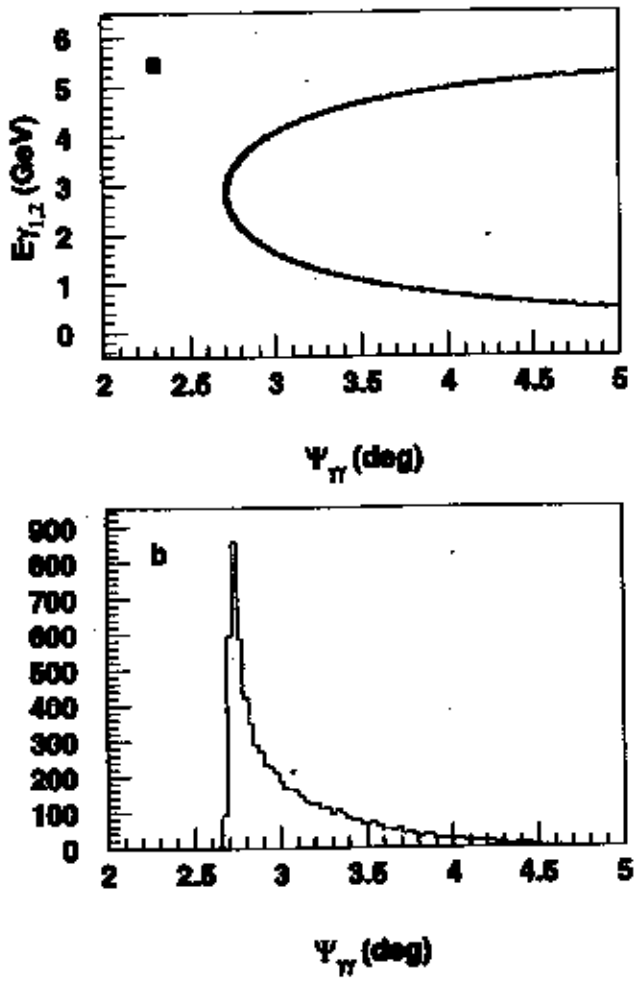

Figure 14. a) Correlation between photon opening angle and two photon energies; b) Opening angle distribution.

shown are for $\Delta\theta_\pi = 0.01°$ bins and are statistical only. A tagged 8×10^6 γ/sec intensity photon beam was assumed for the accepted energy interval $E_\gamma = (0.85 - 0.95)E_o$.

For the first level trigger the last 11 "T" counters of the tagging system will cover this energy range. Therefore, if only "T" counters are used, the expected rate for each channel would be about 1 MHz, which is two times less than the maximum design count rate [24]. The total π° rate in the experiment integrated for the $\theta_\pi = 0° - 2°$ angular interval, and for the parameters listed above is expected to be:

$$Rate = N_\gamma \times N_{nuclei} \times \Delta\sigma \times E_{eff} \approx \tag{12}$$

$$\approx 8 \cdot 10^6 \times 9.2 \cdot 10^{20} \times 2.16 \cdot 10^{-2} \cdot 10^{-27} \times 0.7 = 9600 events/day. \tag{13}$$

The generated angular distributions were fitted with the following procedure: for each $\Delta\theta_\pi$ bin the number of expected events $n_i(\theta_\pi)$ was calculated for each component of the cross

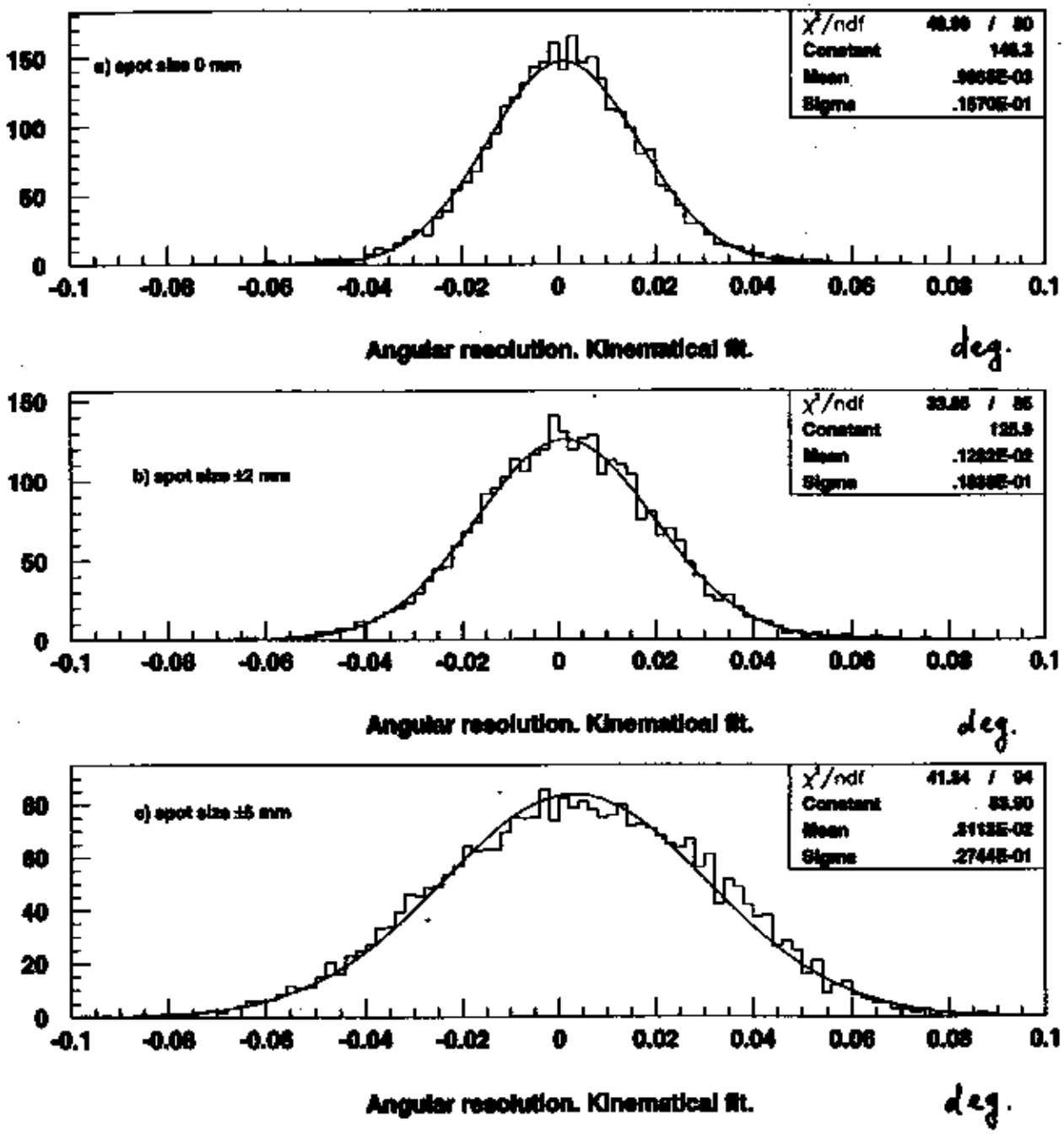

Figure 15. π^o angular resolution for different photon beam spot sizes on the target. Distribution of events *vs.* $(\theta_{\pi^o}^{sampled} - \theta_{\pi^o}^{reconstructed})$ for a) point spot; b) ±2 mm spot size; c) ±5 mm spot size.

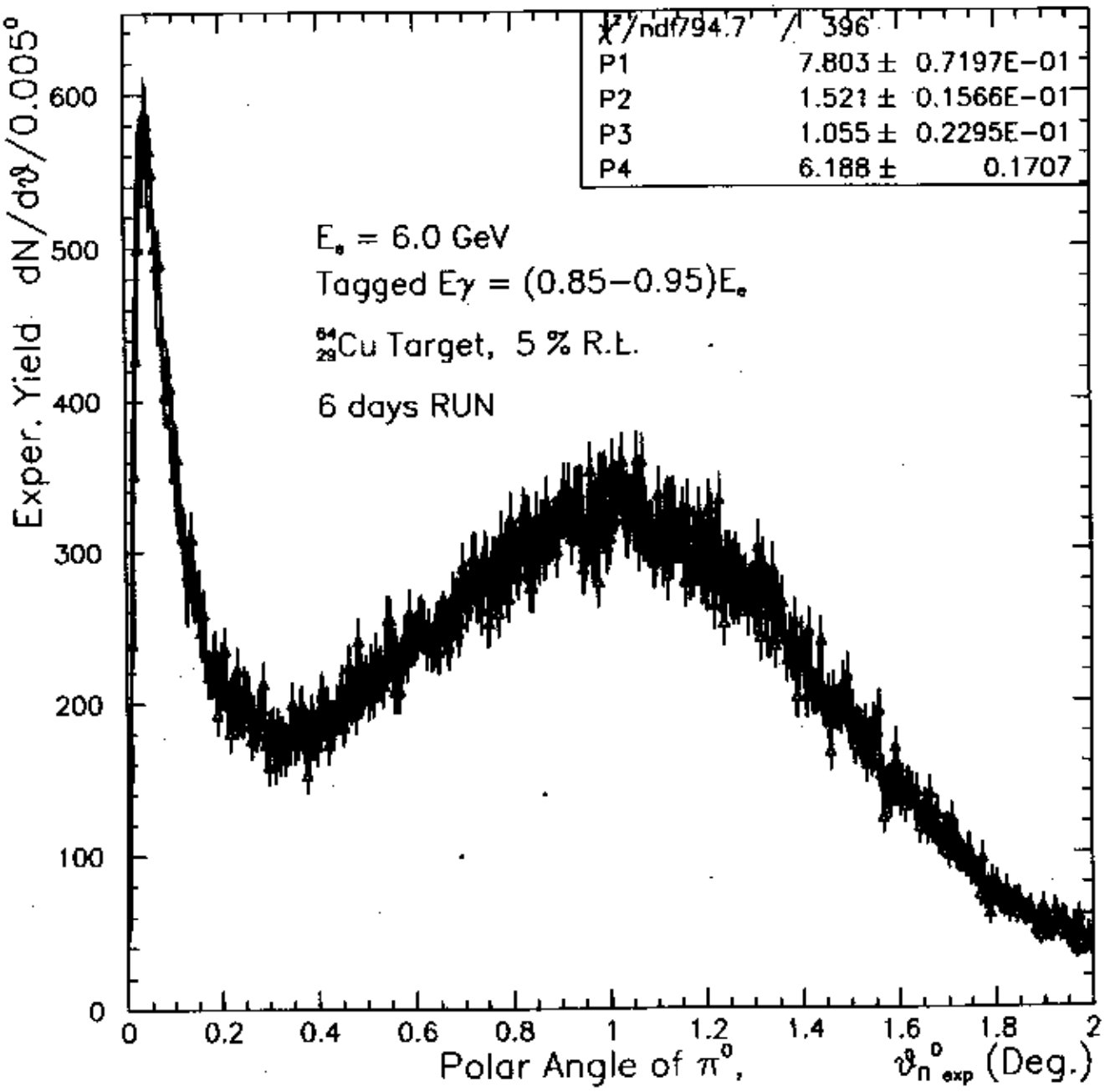

Figure 16. Expected experimental yield vs. θ_{π^0} for 6 days of running on copper.

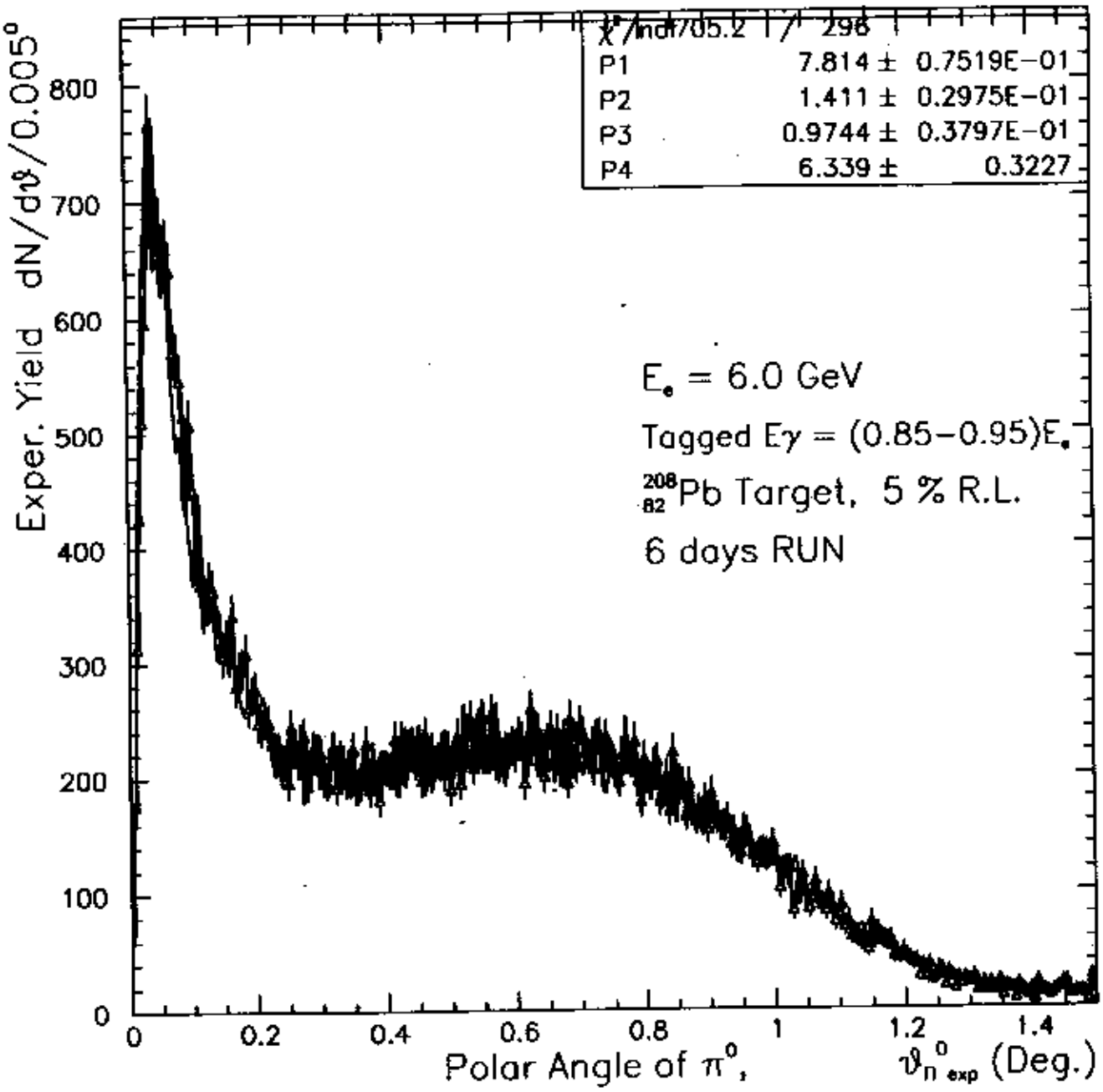

Figure 17. Expected experimental yield *vs.* θ_{π^0} for 6 days of running on lead.

section by folding in the bremsstrahlung spectrum and the detector angular resolution and acceptance. The solid lines on the figures show the result of the fit with the extracted values for all four free parameters. From these data a 0.9% statistical error for the $\pi^o \rightarrow \gamma\gamma$ decay width is achieved. In this energy range the magnitude of the nuclear amplitude is small ($\leq$ 2 %, see figure 3). However, a simultaneous fit of the angular distributions for the two different targets will be used to minimize possible effects depending on the nuclear species.

In addition to the six days of beam time for each target, we estimate three days of beam time for the empty target runs and for the calibration of the multichannel lead glass/$PbWO_4$ detector. Therefore, we estimate a total of 15 days of beam time for the determination of the $\pi^o \rightarrow \gamma\gamma$ decay width with a statistical error less than 1%.

6 π^o background rates

For high photon energies, the dominant photoabsorption mechanism involves the production of the vector mesons ρ, ω, and ϕ. In this experiment, only the ρ and ω decays are expected to produce measurable π^o rates on the detector. The proposed experiment will greatly reduce the uncertainty due to contamination of the Primakoff signal from the other channels for two reasons. First, the proposed hybrid π^o detector consisting of a wall of lead glass detectors and a high resolution insertion will significantly increase pion angular and energy resolutions, thereby enabling tighter cuts on the Primakoff events. Second, the tagging technique provides a powerful kinematical constraint which was not present in previous experiments employing bremsstrahlung beams. The production cross sections for the ω and ρ have been calculated, and their subsequent decays via $\omega \rightarrow \pi^o\gamma$, $\omega \rightarrow \pi^o\pi^-\pi^+$, $\rho \rightarrow \pi^o\gamma$, and $\rho \rightarrow \pi^+\pi^-\pi^o$ have been simulated in GEANT.

The cross section for ω production on complex nuclei is given by:

$$\frac{d\sigma}{dt} = \frac{d\sigma_{A,coh}}{dt} + \frac{d\sigma_{A,incoh}}{dt} \tag{14}$$

The coherent part is given by[25]:

$$\frac{d\sigma_{A,coh}}{dt} = \frac{d\sigma_{Pom}}{dt}(t=0) \cdot e^{Bt} \cdot |A_{eff}^{coh}|^2 \cdot |F(t)|^2 \tag{15}$$

where t is the Mandelstam variable, $\frac{d\sigma_{Pom}}{dt}(t=0)$ is the Pomeron exchange cross section[26], B is taken to be 7 GeV^{-2}[26][27][28], F(t) is the nuclear form factor, and $A_{eff}^{coh} = \sigma_T(\gamma A)/\sigma_T(\gamma N)$ is taken from [29].

The incoherent cross section is given by[25][30]:

$$\frac{d\sigma_{A,incoh}}{dt} = [\frac{d\sigma_{Pom}}{dt} + \frac{d\sigma_{OPE}}{dt}] \cdot A_{eff}^{incoh} \cdot G(t) \tag{16}$$

where A_{eff}^{incoh} is the effective number of nucleons contributing to incoherent vector meson production[29], and G(t) takes into account suppression at small t due to nuclear correlations.

The two body decay $\omega \rightarrow \pi^o\gamma$ (B.R. 8.5×10^{-2}) was sampled in GEANT, with an angular distribution proportional to $(1 + cos^2\theta_{c.m.})$ [31]. The three body $\omega \rightarrow \pi^o\pi^-\pi^+$ decay (B.R. 8.9×10^{-1}) was sampled according to three body phase space. Figure 18(a) shows

the missing energy spectrum ($E_\gamma - E_{\pi^o}$) obtained from the simulation of ω photoproduction and subsequent decay for six days of beam time with a lead target. Since the coherent pion photoproduction will appear as a peak near $E_{miss} = 0$ GeV, figure 18(a) illustrates how knowledge of the incident photon energy provided by the tagging technique enables one to greatly minimize contamination of the π^o spectrum. A further reduction is given by the stringent cut on θ_{π^o} enabled by the high resolution detector insertion. Figure 18(b) shows the angular distribution of π^o's both with and without the four sigma missing energy cut indicated in figure 18(a). As the experimental θ_{π^o} distribution arising from photoproduction via the Primakoff mechanism will be confined to $\theta_{\pi^o} < 0.2^o$, a further substantial reduction in ω background is obtained.

The ρ photoproduction cross section was taken to be ten times the ω cross section[30][32] and the resulting pion detection acceptance from the decays $\rho \rightarrow \pi^o\gamma$ (B.R. 7.9×10^{-4}) and $\rho \rightarrow \pi^o\pi^+\pi^-$ (B.R. $< 1.2 \times 10^{-4}$) were simulated. Figures 19(a) and 19(b) show the resulting missing energy and θ_{π^o} spectra for six days of running on lead, where in figure 19(b), the rates with and without the four sigma missing energy cut are also indicated.

Figure 20 shows the expected total π^o angular distribution for ρ and ω photoproduction, along with the expected yield from the Primakoff mechanism, where missing energy cuts have been imposed.

6.1 Accidentals

Figure 21(a-c) shows the spectrum of single γ events from (a)$\omega \rightarrow \pi^o\gamma$, (b)$\omega \rightarrow \pi^o\pi^+\pi^-$, and (c) the total singles rate from the omega. The singles rates for the ρ were calculated to be 1.4% that of the omega. A summary of the expected singles rates is shown below:

$\omega \rightarrow \pi^o\gamma$	0.12 Hz
$\omega \rightarrow \pi^o\pi^+\pi^-$	0.66 Hz
$\rho \rightarrow \pi^o\gamma$	0.01 Hz
total singles	0.79 Hz
total accidental rate	6.3×10^{-2} Hz
π^o signal rate	0.11 Hz
raw trues/accidentals	1.7

The quoted accidental rate represents raw trigger accidental coincidences between the π^o detector and the photon tagger. When invariant mass, missing energy, and opening angle cuts are applied, the accidentals are expected to be negligible.

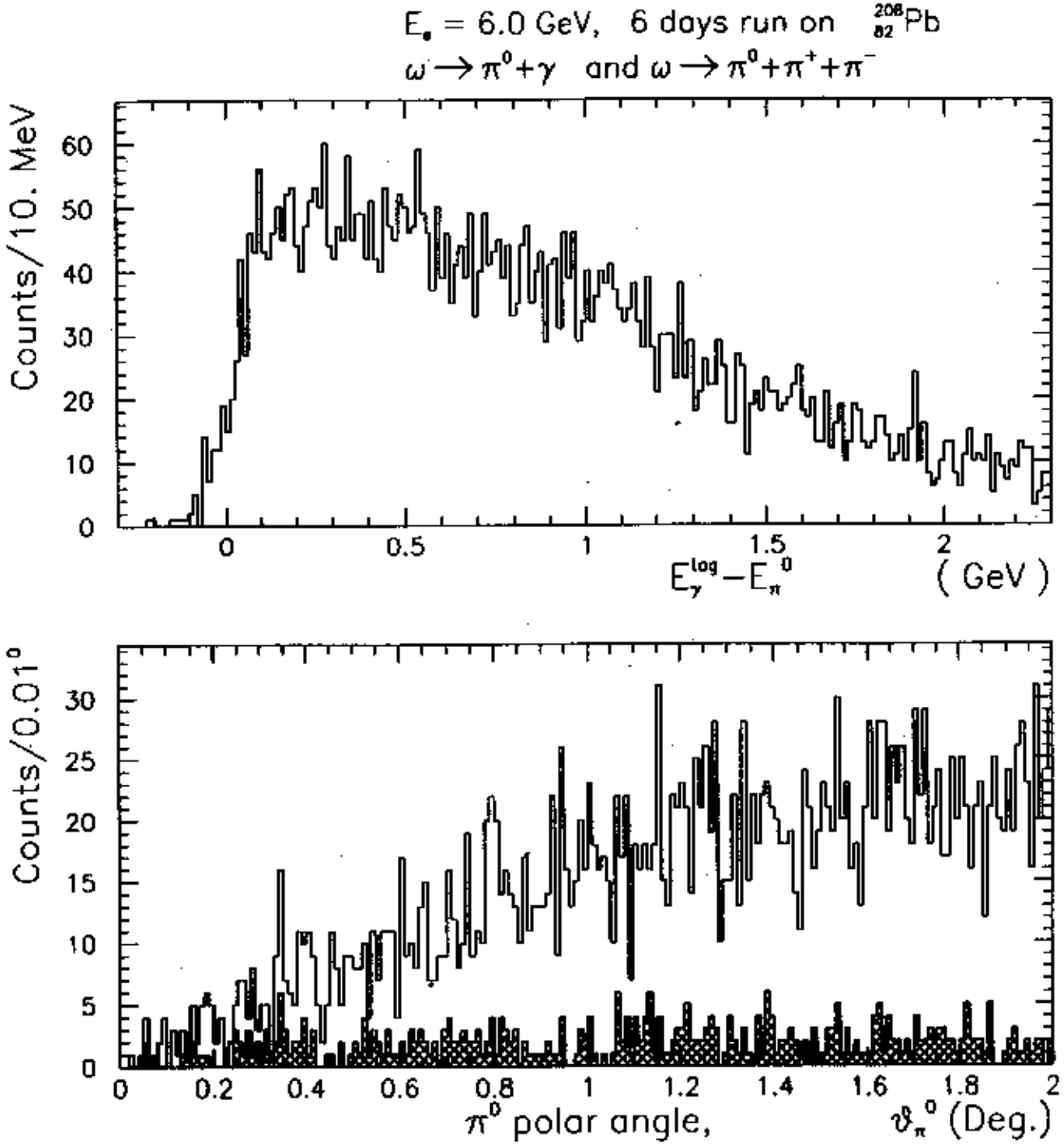

Figure 18. (a) Missing energy spectrum and (b) polar angle spectrum of π^0's from omega decay. Open histograms represent total rates. Cross hatched histogram in (b) represents rates which pass a 4 σ missing energy cut in (a).

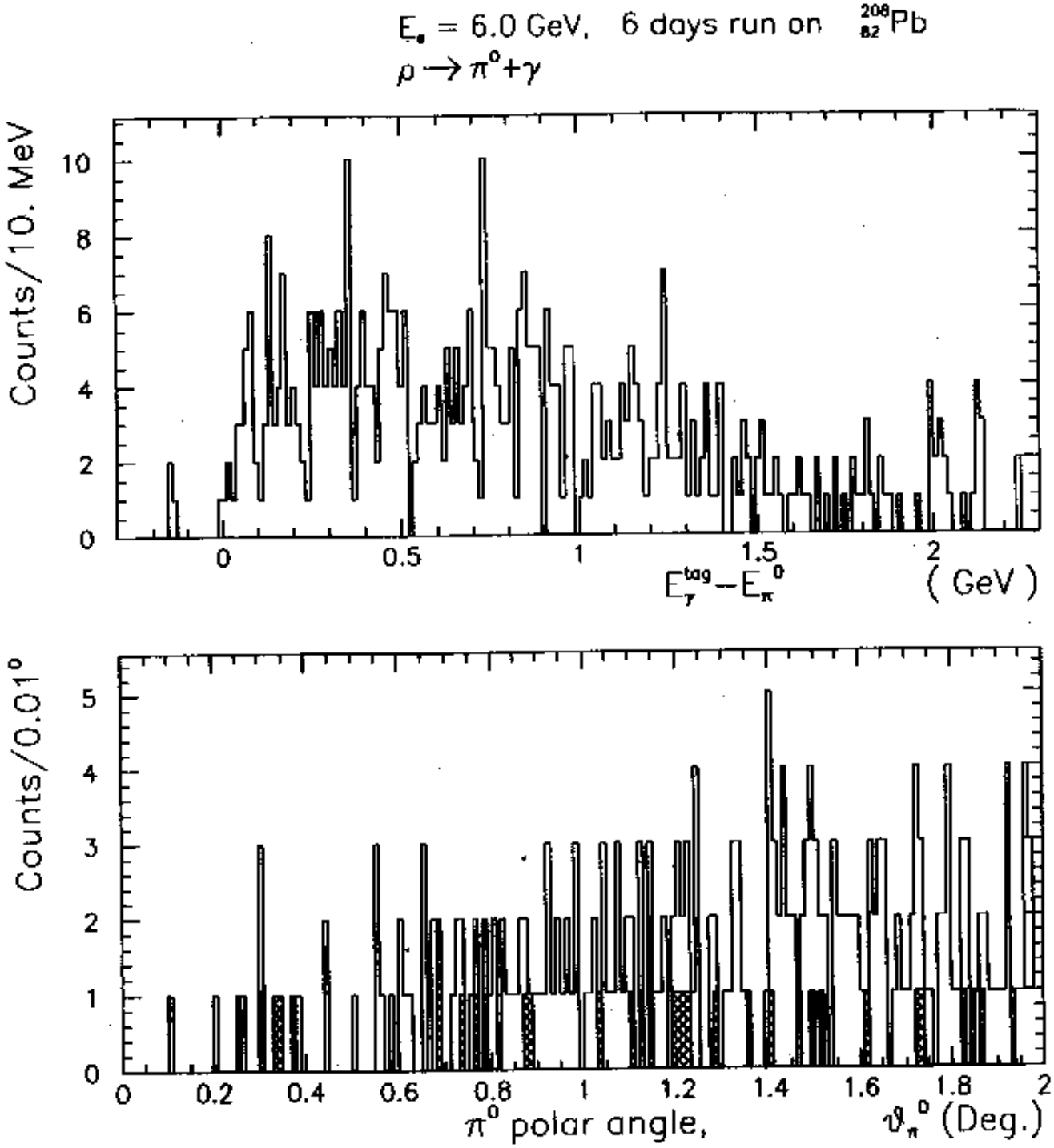

Figure 19. (a) Missing energy spectrum and (b) polar angle spectrum of π^0's from rho decay. Open histograms represent total rates. Cross hatched histogram in (b) represents rates which pass a 4 σ missing energy cut in (a).

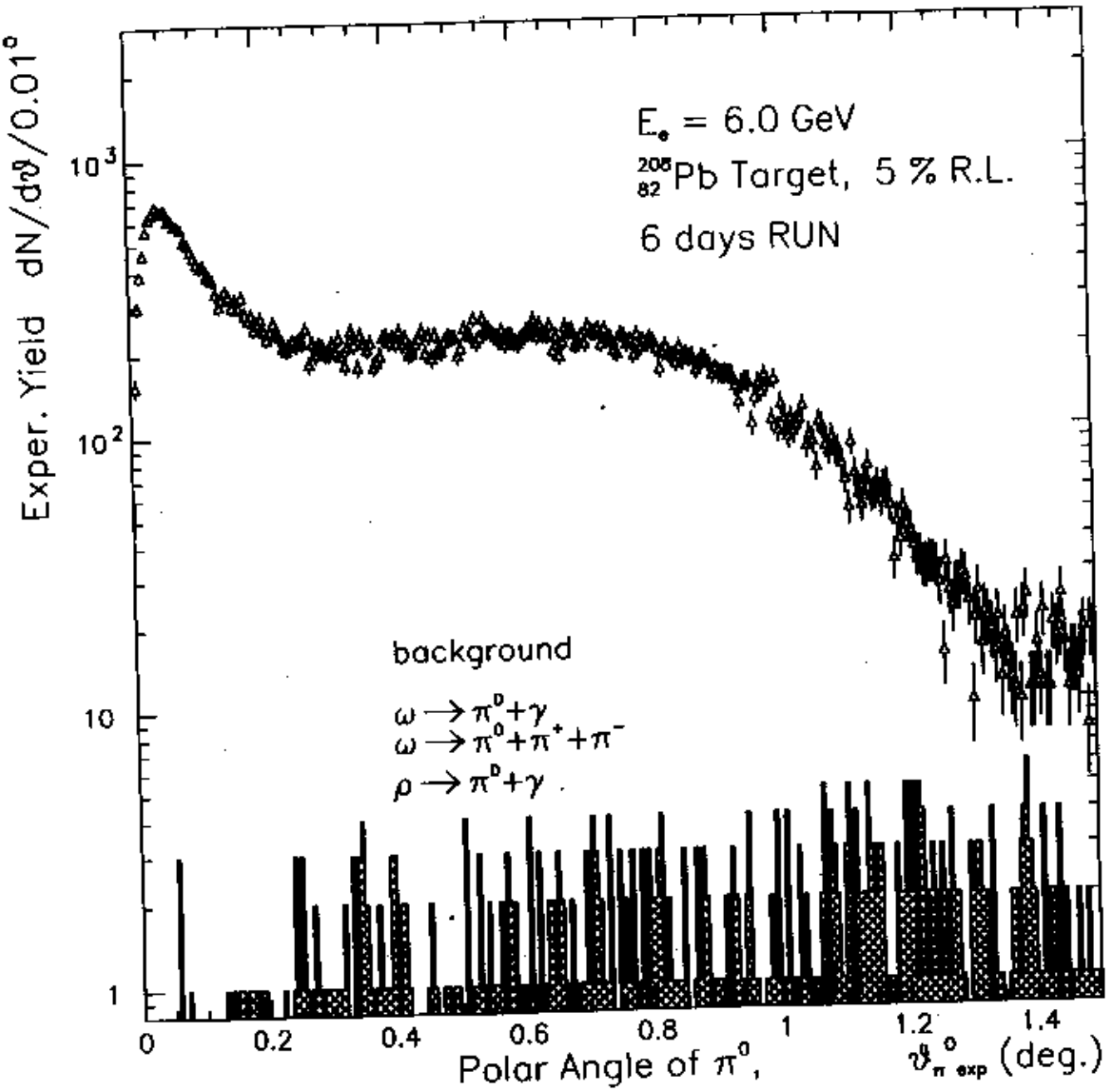

Figure 20. Cross hatched histogram: total π^o background events *vs.* θ_{π^o}. Triangles: Photoproduced π^o's.

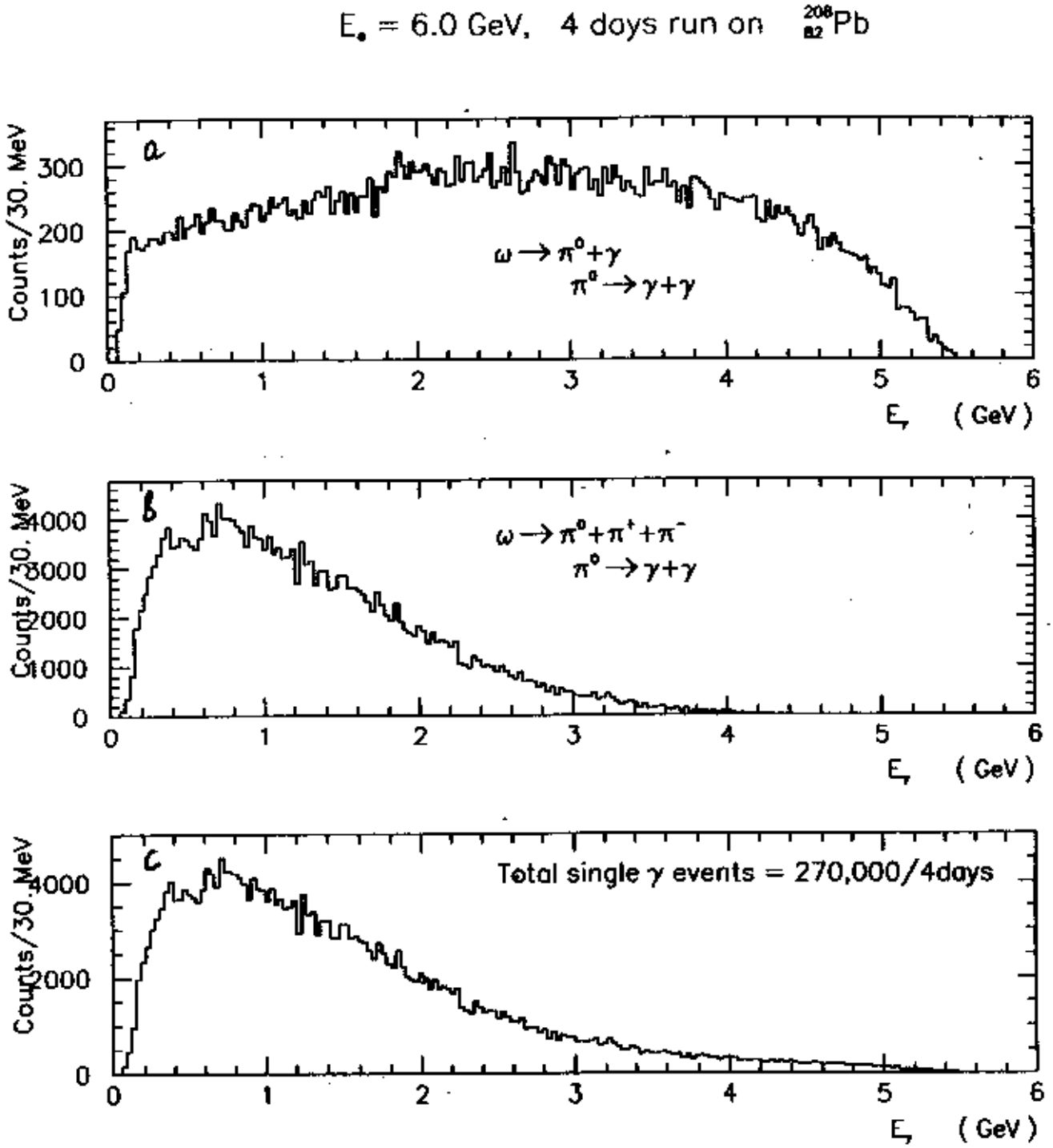

Figure 21. Singles photons expected from four days of running on lead. (a)$\omega \rightarrow \pi^0\gamma$, (b)$\omega \rightarrow \pi^0\pi^+\pi^-$, (c) Total singles from the omega meson.

6.2 Correlated $\gamma\gamma$ backgrounds

The decays $\omega \rightarrow \pi^o\gamma$ and $\rho \rightarrow \pi^o\gamma$ result in three photon states which are correlated in time. Figures 22(a-d) and 23(a-d) show the correlated two photon rates as a function of (a) invariant mass, (b) missing energy, (c) $\psi_{\gamma_1\gamma_2}$, and (d) θ_{π^o}. No cuts are applied in the figures. In figure 22(a), the position and resolution of the π^o invariant mass peak is shown, where the indicated peak height is reduced by a factor of 25 compared to that expected from Primakoff π^o photoproduction. When π^o invariant mass, missing energy, minimum $\gamma_1\gamma_2$ opening angle, and θ_{π^o} cuts are imposed, the correlated background rates are found to be negligible.

7 Experimental uncertainties

We intend to control the experimental errors to make a measurement of the π^o lifetime with a less than 2% precision. The various contributions to this error are shown below:

statistical	0.7%
luminosity	1.4%
π^o detector acceptance and misalignment	0.8%
background subtraction	0.2%
beam energy	0.4%
charge form factor	0.12%
distortion of e.m. form factor	0.5%
total	1.8%

The total error was estimated by adding the individual errors in quadrature. Monte Carlo calculations show that the fitting error on the Primakoff cross section for each target nucleus is expected to be 0.9%. The absolute luminosity will be monitored in two ways: by measuring the tagging efficiency about once per day, and by measuring electron-positron pairs produced in the target during the run. The π^o detector acceptance uncertainty arises primarily from edge effects relating to the position resolution in the blocks near the edges of the detector. In estimating errors in background subtractions, a 30% uncertainty in calculated background π^o's was assumed. The effect of the beam energy uncertainty on the extracted lifetime arises from the E^4 dependence of the Primakoff cross section.

The nuclear form factor will be fit to the data at the larger θ_{π^o}'s and therefore its uncertainty will contribute to the statistical error. Errors in the electromagnetic form factor originate from both uncertainties in the nuclear charge distributions and distortion effects. As can be seen from equation 3, the Primakoff photoproduction cross section is proportional to the square of the nuclear electromagnetic form factor, $|F_{e.m.}(Q^2)|$, where Q is the momentum transferred to the nucleus. The nuclear form factor for ^{208}Pb has been measured over a range of Q^2 to extract the charge density[33][34][35][36][37] [38]. To investigate the uncertainty in

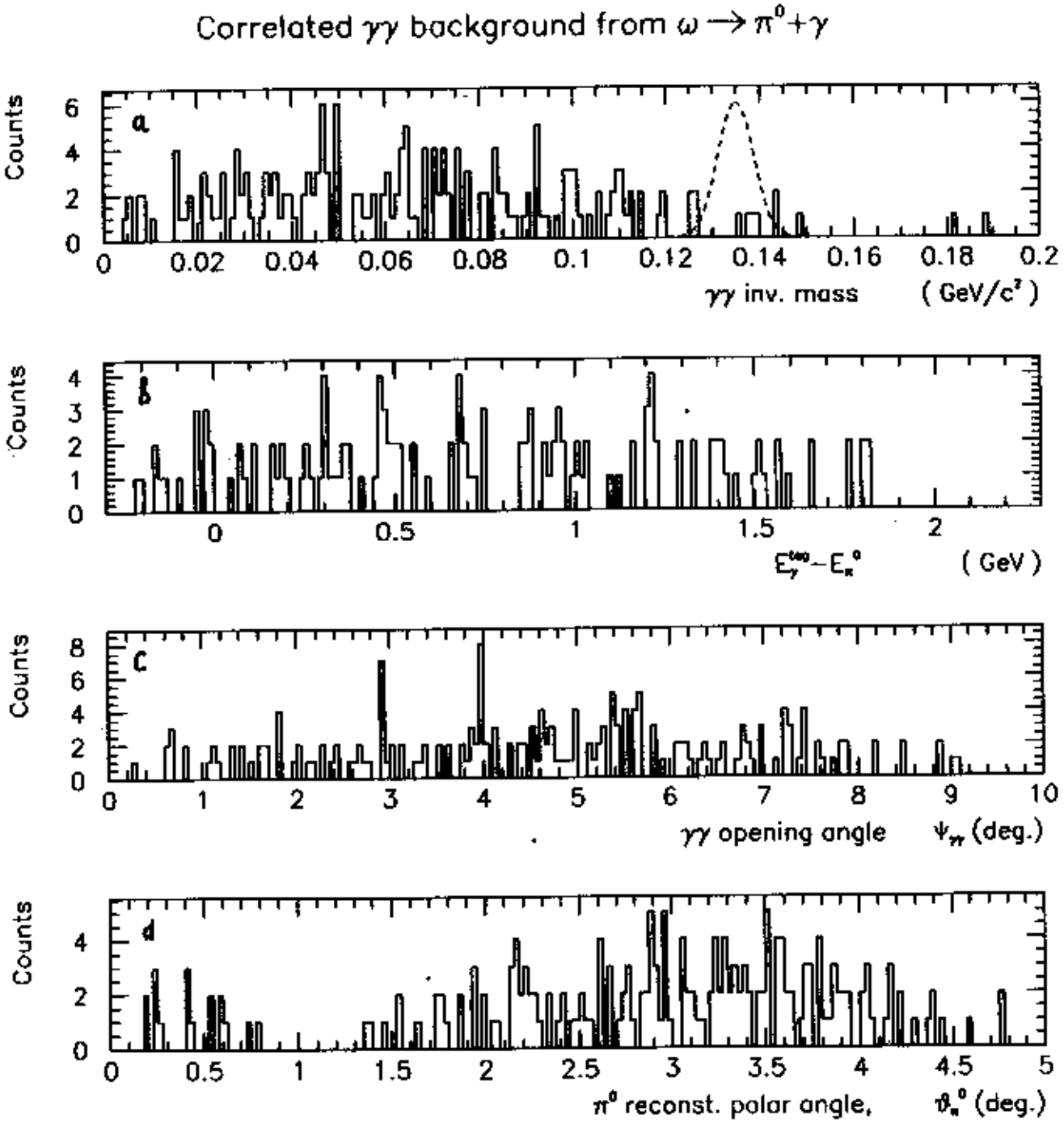

Figure 22. Correlated two photon rates from the omega as a function of (a) invariant mass, (b) missing energy, (c) $\psi_{\gamma_1\gamma_2}$, and (d) θ_{π^0}. No cuts are applied in the figures. In figure (a), the position and resolution of the π^0 invariant mass peak is shown, where the indicated peak height is reduced by a factor of 25 compared to that expected from Primakoff π^0 photoproduction.

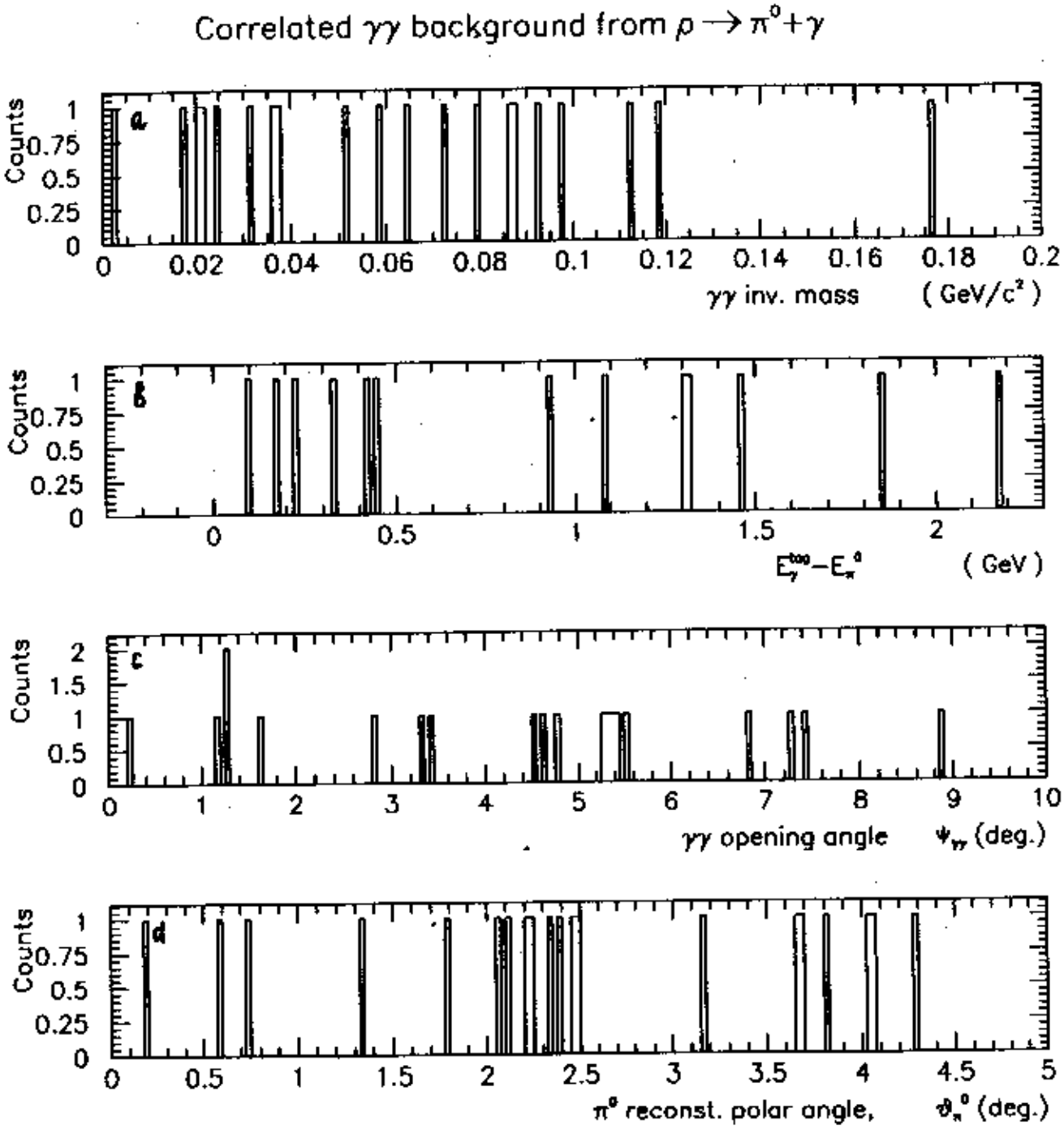

Figure 23. Correlated two photon rates from the rho as a function of (a) invariant mass, (b) missing energy, (c) $\psi_{\gamma_1\gamma_2}$, and (d) θ_{π^0}. No cuts are applied in the figures.

the undistorted electromagnetic form factor in the Q^2 range of the Primakoff peak (0 to 0.1 fm^{-1}), we examined the errors in the parameters of the two parameter Fermi charge distribution of [33]. This resulted in an uncertainty in $|F(q^2)|^2$ of at most 0.12% on the Primakoff cross section. To investigate the sensitivity to the charge parameterization, the form factor was calculated for a uniform sphere while preserving the experimentally measured mean square charge radius. This was found to have a negligible impact on the calculated form factor below momentum transfers of $0.1 fm^{-1}$.

The electromagnetic form factor which modifies the Primakoff cross section (see equation 3) and the nuclear form factor which modifies the coherent pion production cross section (see equation 5) must each be corrected for absorption of the outgoing pion[39][40]. Since the pions from the Primakoff effect are produced peripherally, the effect of pion absorption on the electromagnetic form factor is small. On the other hand, pions produced within the nuclear interior can interact with the nucleus. For the case of lead, absorption results in a nuclear form factor reduction by a factor of about 2.5[16]. As noted in [39], this makes it easier to extract the pion lifetime, as the absorption affects the Primakoff photoproduction very little, but considerably suppresses the coherent nuclear production. Following [39], Omelaenko[41] has calculated both the distorted electromagnetic and nuclear form factors. Figure 24(a) shows the electromagnetic form factor both with and without absorption, plotted in the angular region of the Primakoff peak. As is evident from the calculation, the effect is small, particularly at the low θ_{π^0}'s where the Primakoff cross section is largest. Similarly, figure 24(b) shows the effect of absorption on the nuclear form factor, plotted over the larger range of θ_{π^0} of relevance to nuclear coherent photoproduction. Since the nuclear form factor will be fit to the data, the extrapolation of the nuclear coherent contribution under the Primakoff peak will be largely model independent.

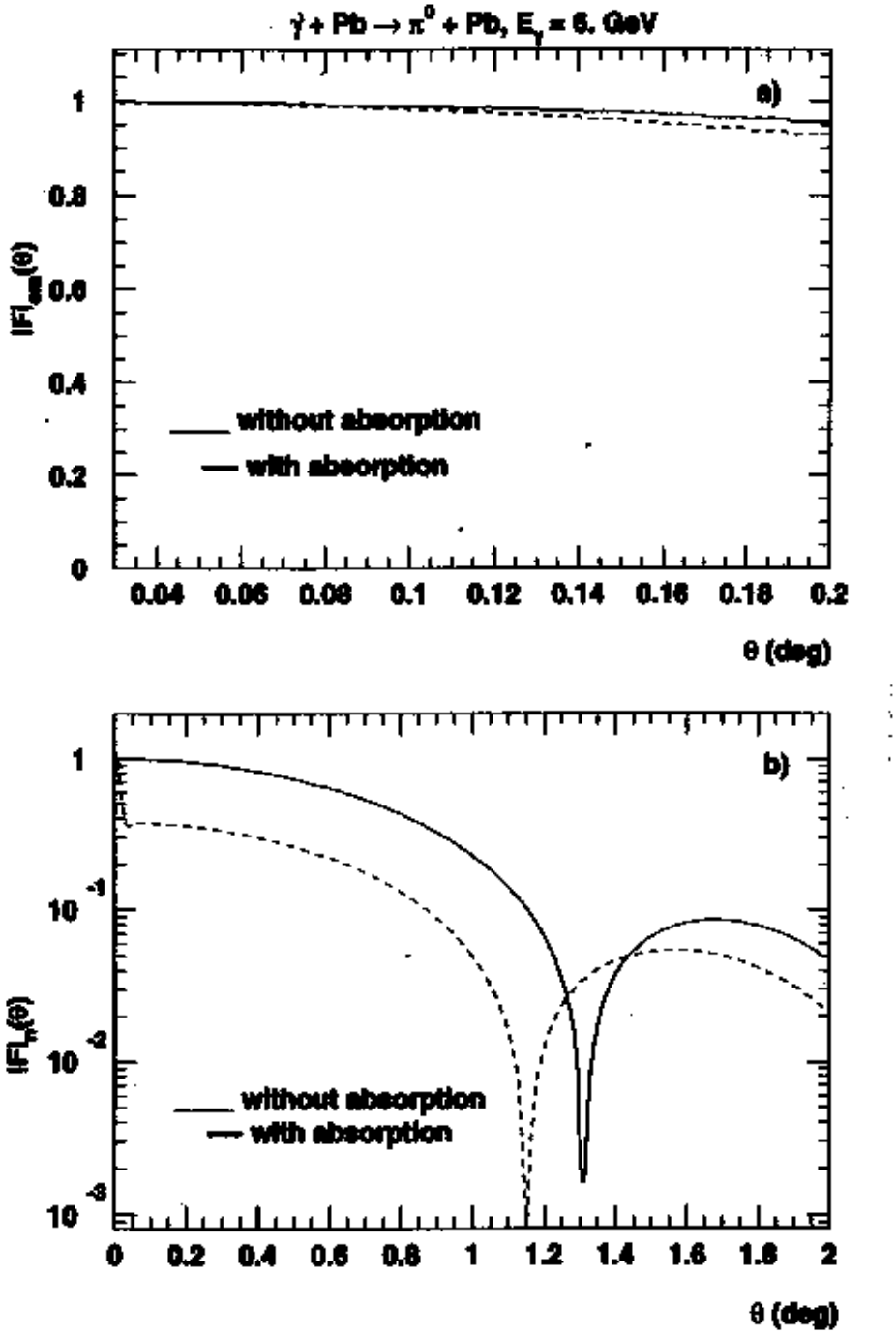

Figure 24.(a) The absolute value of the electromagnetic form factor with and without distortion in the region of the Primakoff peak. (b) The absolute value of the nuclear form factor with and without absorption.

8 Summary

Using the high intensity, high energy photon tagging facility in Hall B of TJNAF, and an array of lead glass detectors with a high resolution $PbWO_4$ crystal insertion, we propose to perform a precise measurement of the neutral pion two photon decay width via the coherent photoproduction of the π^o in the Coulomb field of a nucleus. The tight control of the systematic errors, mainly connected with the superior π^o detection and knowledge of the absolute value of photon energies and fluxes provided by both the high quality TJNAF electron beam and the photon tagging facility in Hall B, is expected to produce an improved measurement which will be of comparable precision to state-of-the-art QCD based theoretical predictions.

We are requesting 15 days of beam time at 6 GeV, six days of data taking each for the Cu and Pb targets, and 3 days of empty target and detector calibration runs. Major new equipment for this experiment includes a multichannel hybrid lead glass/$PbWO_4$ π^o detector and a 15 kilogauss-m dipole magnet for use as a sweeping magnet and pair production luminosity monitor.

References

[1] J.S. Bell et al., Il Nuovo Cimento, vol. 51, no. 1., (1969), 47.

[2] S. Adler, Phys. Rev., vol. 177, no. 5, (1969), 2426.

[3] J. Bijnens, A. Bramon and F. Cornet, Phys. Rev. Lett. 61 (1988) 1453.

[4] J.F. Donoghue, B.R Holstein, Y.C.R. Lin, Phys. Rev. Lett., vol. 55, no. 25, (1985), 2766; J.F. Donoghue, B. Wyler, Nuc. Phys., B316, (1989), 289.

[5] J. Bijnens et al., Z. Phys. C, 46, (1990), 599.

[6] J. Bijens, J. Prades, Z. Phys. C64, (1994), 475.

[7] A.M. Bernstein, Nuc. Phys. A623 (1997) 178c..

[8] R.M. Barnett et al., Review of Particle Physics, Phys. Rev., D54, (1996), 21.

[9] D. Dale, A. Gasparian, Proposal to TJNAF PAC12, E-97-009, (1997).

[10] G. von Darder et al., Phys. Lett., vol. 4, no. 1, (1963), 51.

[11] H.W. Atherton et al., Phys. Lett., vol. 158B, no. 1, (1985), 81.

[12] See, e.g. Dynamics of the Standard Model, J.F. Donoghue, E. Golowich, and B.R. Holstein, Cambridge University Press (1992).

[13] D.A. Williams et al., Phys. Rev. D, vol. 38, no. 5, (1988), 1365.

[14] H. Primakoff, Phys. Rev. 81, 899 (1951).

[15] A. Browman et al., Phys. Rev. Letts., vol. 33, no. 23, (1974), 1400.

[16] G. Bellettini et al., Il Nuovo Cimento, vol. 66, no. 1, (1970), 243.

[17] V.I. Kryshkin et al., Sov. Phys. JETP, vol. 30, no. 6, (1970), 1037.

[18] G. Bellettini et al., Il Nuova Cimento, vol. 40, no. 4, (1965), 1139.

[19] D.I. Sober, A Guide to the Optics of the Tagged Photon Magnet, CLAS Note 91-012.

[20] G.A. Alexeev, *et al.*, NIM A364, (1995), 307.

[21] H. Stroher, G. Koch, V. Metag, R. Beck, B. Schoch, J. Vogt, NIM A269 (1988), 568.

[22] B. Powel et al., Nucl. Instr. and Meth., 198, (1982), 217.

[23] A.S. Aleksanian et al., Preprint YerFI-1239-25-90, (1990).

[24] D.I. Sober, private communication.

[25] T.J. Brodbeck, P. Coddington, J.V. Morris, D. Newton, T. Sloan, Nucl. Phys B136 (1978) 95.

[26] J. Ballam, G.B. Chadwick, Z.G.T. Guiragossian, A. Levy, M. Menke, P. Seyboth, G. Wolf, Phys. Lett., vol. 30B, no. 6 (1969) 421.

[27] Y. Eisenberg, B. Haber, Carmel, E. Peleg, E.E. Ronat, A. Shapira, G. Vishinsky, R. Yaari, G. Yekutirli, Phys. Rev. Lett., vol. 22, no 13 (1969) 669.

[28] Y. Eisenberg, B. Haber, E.E. Ronat, Y. Stahl, G. Yekutirli, J. Ballam, G.B. Chadwick, M.M. Menke, P. Seyboth, A. Shapira, J. Gandsman, J. Grunhaus, A. Levy, Phys. Lett, vol. 34B, no. 5 (1971) 439.

[29] D.O. Caldwell, V.B. Elings, W.P. Hesse, R.J. Morrison, F.V. Murphy, Phys. Rev. D, vol. 7, no. 5 (1973) 1362.

[30] T.H. Bauer, R.D. Spital, D.R. Yennie, Rev. Mod. Phys., vol. 50, no. 2 (1978) 261.

[31] P.L. Braccini, C. Bradaschia, R. Castaldi, L. Foa, K. Lubelsmeyer, D. Schmitz, Nucl. Phys. B24 (1970) 173.

[32] H.-J. Behrend, F. Lobkowicz, E.H. Thorndike, A.A. Wehmann, Phys. Rev. Lett., vol 24, no. 22 (1970) 1246.

[33] de Jager, de Vries, deVries, At. Data and Nuc. Data Tables, vol. 14, no. 5 (1974) 480.

[34] J.B. Bellicard and K.J. van Oostrum,Phys. Rev. Lett., vol. 19, no. 5, (1969) 242.

[35] G.J.C. van Niftrik, Nuc. Phys. A131, (1969), 574.

[36] J. Heisenberg, R. Hofstader, J.S. McCarthy, I. Sick, B.C. Clark, R. Herman, D.G Ravenhall, Phys. Rev. Lett., vol. 23, no. 24. (1969),1402.

[37] J. Friedrich, F. Lenz, Nuc. Phys. A183 (1972), 523.

[38] H. Euteneuer, J. Friedrich, N. Voegler, Phys. Rev. Lett., vol. 36, no. 3, (1976) 129.

[39] G. Morpurgo, Nuovo Cimento, 31, (1964), 569.

[40] C.A. Engelbrecht, Phys. Rev. 133, (1964), 988.

[41] A. Omelaenko, private communication, 1998.